CHALMERS

Ringhals Diagnostics and Monitoring, Annual Research Report 2022-23:

Analysis of the vibrations of thimble tubes by wavelet techniques

I. PÁZSIT
V. DYKIN
H. NYLÉN

Nuclear Engineering Group
Division of Subatomic, High Energy and Plasma Physics
CHALMERS UNIVERSITY OF TECHNOLOGY
Gothenburg, Sweden, 2023
CTH-NT-349/RR-26 June 2023

CTH-NT-349/RR-26 June 2023

Ringhals Diagnostics and Monitoring, Annual Research Report 2022-2023:

Analysis of the vibrations of thimble tubes by wavelet techniques

I. Pázsit, V. Dykin and H. Nylén

Nuclear Engineering Group
Division of Subatomic, High Energy and Plasma Physics
Chalmers University of Technology
SE-412 96 Göteborg, Sweden
ISSN 0281-9775

Ringhals Diagnostics and Monitoring, Annual Research Report 2022-2023:

Analysis of the vibrations of thimble tubes by wavelet techniques

I. Pázsit, V. Dykin and H. Nylén

Nuclear Engineering Group
Division of Subatomic, High Energy and Plasma Physics
Chalmers University of Technology
SE-412 96 Göteborg, Sweden

Abstract

This report gives an account of the work performed by the Division of Subatomic, High Energy and Plasma Physics (formerly, Division of Nuclear Engineering), Chalmers, in the frame of a research collaboration with Ringhals, Vattenfall AB, contract No. 4501756928-062. The contract constitutes a one-year co-operative research work concerning diagnostics and monitoring of the PWR units. The work in the contract has been performed between 1 July 2022 and 30 June 2023. During this period, we worked with one single item, namely with the analysis of in-core measurements with wavelet techniques, to detect and quantify thimble tube vibrations.

The work was performed by Imre Pázsit (project leader at Chalmers), Victor Dykin and Henrik Nylén, the latter being the contact person at Ringhals.

CONTENTS

1. INTRODUCTION

This report gives an account of the work performed by the Division of Subatomic, High Energy and Plasma Physics (formerly, Division of Nuclear Engineering), Chalmers, in the frame of a research collaboration with Ringhals, Vattenfall AB, contract No. 4501756928-062. The contract constitutes a one-year co-operative research work concerning diagnostics and monitoring of the PWR units. The work in the contract has been performed between 1 July 2022 and 30 June 2023. During this period, we worked with one single item, namely with the analysis of in-core measurements with wavelet techniques, to detect and quantify thimble tube vibrations.

A separate report, giving an overview of the nearly 30 years of collaboration, is submitted simultaneously with this report.

The work was performed by Imre Pázsit (project leader at Chalmers), Victor Dykin and Henrik Nylén, the latter being the contact person at Ringhals.

2. ANALYSIS OF THE VIBRATIONS OF THIMBLE TUBES WITH WAVELET TECHNIQUES

2.1 Preliminaries

The phenomenon of thimble tube vibrations, and the possible consequences of these vibrations and impacting of the thimble tubes on the instrument tubes have long been known. The problem got a wider attention first within the nuclear program of EDF in the late 1980's, when their 1300 MWe PWR plants were introduced [1, 2]. Several cases of thimble tube vibrations and their effects were observed, including fatigue and wear of both the thimble tube and the instrument tube, and in some cases leaks in the thimble tube. This resulted in the fact that EDF launched a dedicated program for the surveillance and monitoring of thimble tube vibrations and impacting [3].

The investigation of possible thimble tube vibrations was taken up within the Chalmers-Ringhals collaboration in Stage 2018 [4], when also a survey of the literature on the previous experiences was performed. This problem was new to us, without having previous experience. There is also rather little help in the literature. The most effective method recommended by EDF was to use ex-core accelerometers, attached to the guide tubes below the bottom of the pressure vessel. These accelerometers can detect both the vibrations (from the periodic component of the signal) as well as impacting (from the spikes caused by the impacting). Unfortunately, this possibility is not available in Ringhals, due to the absence of such accelerometer signals. The only tool which can be used is the in-core neutron noise measurements.

Apart from a very few in-core noise measurements in the Ringhals PWRs, we have had very little experience with diagnosing in-core PWR vibrations, in particular when vibrations of the detector itself were involved. The closest problem with some resemblance to the thimble tube vibrations is the detector instrument tube vibrations and impacting in BWRs [5]. BWR instrument tube vibrations can also lead to impacting against the wall(s) of some of the surrounding four fuel boxes. In some cases heavy impacting led to damage of the LPRM detectors in the instrument tube, and even to holes in the fuel channel walls, leading to undesired cross-flow. Such instrument tube vibrations and impacting have occurred also in Swedish BWRs [5], and the problem was investigated in several previous Stages, i.e from Stage 8 through Stage 12 [6, 7, 8, 9, 10], as well as in some stages of the SKI reports [11, 12, 13]. A summary of these investigations is found in the companion report "Ringhals Diagnostics and Monitoring: An overview of 30 years of collaboration 1993 - 2023", Section 2.4 [14].

As is described in the above mentioned publications, there are several tools and possibilities for the detections BWR instrument tube vibrations from the in-core neutron noise. Originally spectral and correlation methods were used. The vibration of the detectors could be observed from the small peaks in the detector

APSDs; in case of stronger vibrations the coherence and phase between detectors in the same detector tube started deviating from the typical pattern of the vibration-free case, where the phase is a linear function of the frequency, and the coherence shows a regular sink-peak structure. A large deviation from this pattern, as well as a widening of the peak in the APSD was an indication of the increased possibility of impacting.

All the above features serve though only as indirect indicators of impacting, which is the main matter of interest. We found a better method which could be a direct indicator of impacting in wavelet methods. The idea is based on a hypothesis of J. Thie [15]. Thie suggested that the impacting of the detector tube on the fuel channel box should induce short, damped oscillations of the fuel box itself, presumably with a higher frequency as the eigenfrequency of the detector tube vibrations, which would manifest itself as a 'spike" in the detector signal. Alternatively, the impacting could induce higher order vibration modes of the detector tube itself, which would be damped much stronger than the fundamental mode, hence they also would die out fast and would manifest themselves as spiker. In either way, impacting can expected to lead to spikes in the detector signal, thus detection of impacting could be performed by finding such spikes. Then the frequency of their intermittent occurrence would indicate the severity of impacting. The problem boils down to find and extract such spikes from a noisy signal, where they are not visually visible.

Wavelet analysis, via wavelet filtering, lends a possibility to find such spikes in a noise signal. The essence is to perform a discrete wavelet transform, which generates the signal as a sum of scaled and shifted versions of the mother wavelet, then setting the components whose coefficient is below a given threshold, to zero, and perform an inverse wavelet transform back to time domain. With a proper choice of the threshold for the filtering, the wavelet filtered time signal contains only the spikes.

This method was first tried with Haar wavelets, and was tested on the old Barsebäck measurements, were one had access to signals both with and without impacting. The test was successful, i.e. the wavelet filtering showed a manifold time more spikes for an impacting detector than for a on-impacting detector [16]. Later on this method was developed further, such as using different thresholds for the different levels of the transformed signal, and as an alternative method, wavelet-based coherence was also used. In the discrete wavelet transform, the so-called impacting rate (IR) was introduced, which expresses the number of spikes per unit time. The continuous wavelet-transform based coherence was taken between detector 2 and 4 of the same string, but there was no quantitative indicator, only a visual plot of the results.

When taking up the problem of thimble tube vibrations, we tried to draw from our previous experience from BWR tube vibrations, as well as some other experience with vibrating absorbers we had outside the Ringhals project [17, 18]. This latter is because the thimble tube vibrations are somewhat in beween tbe BWR detector tube vibrations and the PWR in-core vibrations such as that of control rods. One difference to the BWR case is that each of the 36 instrument tubes whose vibrations have to be monitored are equipped by four LPRM detectors. Therefore the vibrations/impacting can be studied through the signals of the vibrating

detectors themselves. In the case of the thimble tubes, only signals of a total of four in-core detectors are available at four different radial positions, whereas many other thimble tubes, not housing a detector, might vibrate. This latter case is then similar to finding a vibrating absorber from the signals of detectors apart from the vibrating thimble tube. Whereas the cross-correlation between two detectors in the same BWR instrument tube yield information on the detector tube itself, the cross-correlation between two in-core detectors at two different radial position in a PWR might carry information about a thimble tube in a third position. Also the possibility of cross-correlating two detector in the same radial but different axial position is missing.

A general difficulty with the diagnostics of thimble tube vibrations with neutron noise is that the signal to background noise ratio is presumably small, and the eigenfrequency of the thimble tube vibrations is not known. The low signal to noise ratio follows from the fact that the amplitude of the vibrations is smaller for thimble tubes than for BWR instrument tubes (which are situated in between four fuel elements) and the flux gradient in which the detector moves is also smaller for detectors in the thimble tubes than for BWR detector tubes. The neutron noise from thimble tube vibrations as a perturbation is also low because the thimble tubes constitute a much weaker absorber than a control rod.

The first attempt to diagnose thimble tube vibrations was made during Stage 2018 [4]. In that year, no new in-core measurements were possible to make, hence we decided to use the in-core measurements analysed in Stage 12 for fuel assembly vibrations, taken in 2008, in cycle 25 in R4. By the time of Stage 2018, the previous experience by wavelet methods was lost, hence those measurements were only analysed by spectral and correlation methods. Due to the above described circumstances, the spectral methods are not very effective for thimble tube vibrations, and correspondingly, no clear-cut decision was possible to be drawn from the analysis.

New measurements were planned during Stage 2019, but these could not be performed, due to the pandemics, and during that Stage no investigation of thimble tube vibrations was made. The first time new measurements were made was during Stage 2020, on 1 December 2020. Two measurements were made, one at six axial levels with a 30-minute recording at each level, and one consisting of measurements in 21 axial points, with a one-minute measurement in each point. Especially the second of these two measurement were made in view of wavelet analysis. However, recovering the wavelet method took longer than expected, and only Measurement 1 was evaluated with spectral and correlation methods. Within the possibilities and limitations of the spectral methods, no evidence was found for thimble tube vibrations in positions which did not contain detectors. Regarding the positions containing detectors, three thimble tubes could be suspected for vibrations, but no definite statement on possible impacting could be made [19]. This further amplified the need for the re-introduction of wavelet-based methods.

In Stage 2021, yet another pair of new measurements were made in R3, with two different layouts (similar to those in the preceding stage) on 8 April 2022. Although the measurements were made in 2022, they will be referred to as "the measurements in Stage 2021". The first measurement, taken at 6 (+1 extra) axial positions was

analysed by spectral methods. The second measurement, where the detectors were moved across the axial extension of the core in 21 steps, therefore being close to a uniform movement of the detectors, was evaluated by continuous wavelet transform (CWT). This is still not the wavelet filtering method, which gives a statement on the likelihood of impacting; it only gives a visual presentation from which a subjective judgement on the likelihood of impacting can be drawn.

The introduction of the previously used most effective techniques, namely the discrete wavelet transform (DWT) based wavelet filtering method, and the CWT based coherence method, was left to the present Stage. Unlike the continuous wavelet transform used in Stage 2021, these new methods are suitable to analyse the measurements with 6 levels and longer recording times, i.e. Measurement 1. With the newly implemented methods, Measurement 1 from both Stage 2020 and 2021 were evaluated, and the results are described in this report.

In the following, first the principles of the wavelet based methods will be briefly summarised. Then the layout of the measurements from both Stages 2020 and 2021 will be described. Finally the analysis results will be reported and discussed.

2.2 General principles

2.2.1 Wavelet filtering with discrete wavelet transform

A discrete wavelet function at scale m and location n is defined as [20]

$$\psi_{m,n}(t) = \frac{1}{\sqrt{m}}\,\psi\left(\frac{t-n}{m}\right) \tag{2.1}$$

where m and n are discrete numbers, and $\psi(t)$ is called the *mother wavelet*. In practice, instead of integer numbers, the dilatation and translation parameters are rather chosen via a logarithmic scaling, such that

$$\psi_{m,n}(t) = \frac{1}{a_0^{m/2}}\,\psi\left(a_0^{-m}\,t - n\,b_0\right) \tag{2.2}$$

where now m and n are integers, whereas a_0 and b_0 are the dilatation and translation constants. The standard choice is to use $a_0 = 2$ and $b_0 = 1$, which will be used in the continuation.

A discrete wavelet transform of a function $f(t)$ consists of calculating the wavelet coefficients $T_{m,n}$ as

$$T_{m,n} = \int_{-\infty}^{\infty} f(t)\,\psi_{m,n}(t)\,\mathrm{d}t \tag{2.3}$$

where the $T_{m,n}$ are the wavelet coefficients.

If the wavelets are orthonormal, then, similarly to a discrete Fourier transform, the original time series can be represented with a double infinite sum of the dilated and translated wavelet functions, multiplied by the corresponding coefficients:

$$f(t) = \sum_{m=-\infty}^{\infty}\sum_{=-\infty}^{\infty} T_{m,n}\,\psi_{m,n}(t) \tag{2.4}$$

The simplest form of wavelet filtering, which enhances the presence of spikes (i.e. short lived transients) is performed with a so-called denoising. This is performed such that all coefficients $T_{m,n}$ that are smaller than a given threshold, are set equal to zero in (2.4). That is, one defines the coefficients $T^{\tau}_{m,n}$ such that

$$T^{\tau}_{m,n} = \begin{cases} T_{m,n} & \text{if} \quad |T_{m,n}| \geq \tau \\ \\ 0 & \text{otherwise} \end{cases} \tag{2.5}$$

and reconstructing the wavelet filtered time signal $f^{\tau}(t)$ as

$$f^{\tau}(t) = \sum_{m=-\infty}^{\infty} \sum_{=-\infty}^{\infty} T^{\tau}_{m,n}\, \psi_{m,n}(t) \tag{2.6}$$

where τ is the filter threshold. Much of the success of the filtering depends on the proper choice of the threshold, which in its term depends on the properties of the noisy signal and the transient, which are usually not known. Hence application of the method requires some experimenting. Usually, the variance of the background noise is used to set the threshold in an algorithmic way. The background noise level, on its turn, is determined from the high frequency tail of the APSD, for frequencies above the eigenfrequency of the transient (the fuel assembly vibrations, or the higher harmonics of the detector tube on impacting). In addition, in the recent Matlab routines of de-noising, there are in-built automatic methods to select the proper threshold.

A more advanced method of wavelet filtering method is that instead of taking the "pure" wavelet transform, Eq. (2.3) to represent the original signal via (2.4), to divide the original signal to approximations and details of different scales with a so-called multiscale resolution. This is achieved by the help of the co-called scaling function (or father wavelet) $\phi_{m,n}(t)$ where

$$\phi_{m,n}(t) = 2^{-m/2}\, \phi(2^{-m\,t} - n) \tag{2.7}$$

with the property

$$\int_{-\infty}^{\infty} \phi_{0,0}(t)\, \mathrm{d}t = 1 \tag{2.8}$$

Then, the approximation coefficients $S_{m,n}$ are defined as

$$S_{m,n} = \int_{-\infty}^{\infty} f(t)\, \phi_{m,n}(t)\, \mathrm{d}t \tag{2.9}$$

One can then get the approximations and details of the original time signal $f(t)$ at scale index m as

$$f_m(t) = \sum_{n=-\infty}^{\infty} S_{m,n}\, \phi_{m,n}(t) \tag{2.10}$$

The details d_m of $f(t)$at scale m are defined as

$$d_m(t) = \sum_{n=-\infty}^{\infty} T_{m,n}\, \psi_{m,n}(t) \tag{2.11}$$

It can then be shown that the original signal can be written in terms of approximations and details as

$$f(t) = f_M(t) + \sum_{m=-\infty}^{M} d_m(t). \tag{2.12}$$

Often $M = 1$ is chosen, in which case in the representation of the original signal there is one approximation $f_1 = A$ and a sum of details. This constitutes the multiscale resolution of the original signal. The development from the "simple" wavelet filtering means to choose different thresholds for the coefficients at the different details (scales). Finally, after the denoising of the details by wavelet filtering, the largest scale approximation A is subtracted from the wavelet denoised signal $Den(f)$, i.e. using

$$V(t) = Den(f) - A \tag{2.13}$$

for the further analysis

The signal $V(t)$ generated by the above procedure contains the spikes which are supposed to indicate impacting. We defined the impacting rate (IR index) as the number of spikes found in $V(t)$ per unit time. This can be calculated algorithmically and presented together with the figure of the wavelet filtered signal, as will be shown in the next Section.

This method was implemented in a Matlab program, originally developed in Stage 9 by Carl Sunde, and was used in the evaluation of the measurements.

2.2.2 Wavelet coherence with continuous wavelet transform.

This method is based on a suggestion which was originally developed for a loose parts monitoring system [21]. In Stage 9 it was adopted for surveillance of BWR detector tube vibrations. In analogy with the traditional spectral analysis method, the wavelet coherence was calculated between the signals of two detectors in the same instrument tube. The wavelet coherence between two signals $\phi_1(t)$ and $\phi_2(t)$ is determined as follows. First a short-term averaging integral of the wavelet transforms is calculated as

$$C^w_{1,2}(f,t) = \int_{t-\frac{T}{2}}^{t+\frac{T}{2}} W_1^*(f,\tau)\, W_2(f,\tau)\, \mathrm{d}\tau \tag{2.14}$$

where the $W_i(f,\tau)$, $i = 1, 2$ are the continuous wavelet transforms of the signals $\phi_1(t)$ and $\phi_2(t)$, respectively. Since we are dealing with time-dependent processes, instead of using the scale, the continuous wavelet transform is a function of frequency and time. The averaging interval T is chosen to be 100 times the sampling time increment (inverse of the sampling frequency), in order to get a proper averaging. The frequency-time dependent wavelet coherence $\mathrm{Coh}^w_{1,2}(f,t)$ is then calculated as

$$\mathrm{Coh}^w_{1,2}(f,t) = \frac{|C^w_{1,2}(f,t)|}{\sqrt{C^w_{1,1}(f,t)\, C^w_{2,2}(f,t)}} \tag{2.15}$$

This method was also developed in Stage 9, and was used for analysing measurements in Stage 12 for BWR instrument tube impacting. The motivation for this method

is as was shown in [21], that the wavelet coherence can identify characteristics at certain frequencies that cannot be seen in the spectral functions (APSD) or the wavelet-based spectrograms of single signals.

It has to be noted though, that the application in the BWR case is much more straightforward, since it concerns the coherence between two detectors in the same instrument tube, hence it supplies information solely on the detector string in question. Since in the case of thimble tube vibrations, the coherence is taken between two detectors in two different thimble tubes, the information content of the wavelet coherence is not clear. It can carry information on either of the thimble tubes, or a thimble tube in between, or close to, the two thimble tubes with a detector. Hence in this report the wavelet coherence method is rather used to test the potentials of its use.

2.3 The layout and details of the measurements

In this report the measurements made in both Stage 2020 and 2021 will be evaluated with the new wavelet based methods. In the continuation the measurements in Stage 2020 and Stage 2021, for simplicity they will occasionally be referred to as the "2020" and "2021" measurements, although the measurement in Stage 2021 was made in 2022. The layout of the measurements was identical in the two cases. In both Stages, four movable in-core detectors were used, labelled from A to D, in the same core positions. The detector notations with their corresponding core positions are shown in Table 2.1 and Fig. 2.1.

In-core detector	Core position
A	N12
B	N08
C	N10
D	L04

Table 2.1: The detector designations in the instrumented thimble tubes and their core positions.

As it is seen from the core map and from Table 2.1, the in-core detectors are aligned nearly along a line (in column N of the core, except detector D). Originally, detector D was intended to be placed into the core position N05, but this position shares the guide tube switch with position N12, which is already used in the measurement, this is why position L04 was chosen for detector D. Due to the placing of the detectors, in the coherence and phase analysis, one expects information on the possible vibrations of thimble tubes in column N or its neighbourhood.

What regards the axial positions of the detectors, measurements were made in a number of axial positions during a given time simultaneously for all four detectors. After the measurement at the first level, all detectors were made simultaneously to the next level. In both stages there were two measurement series with two different arrangement of the axial detector positions and corresponding measurement times,

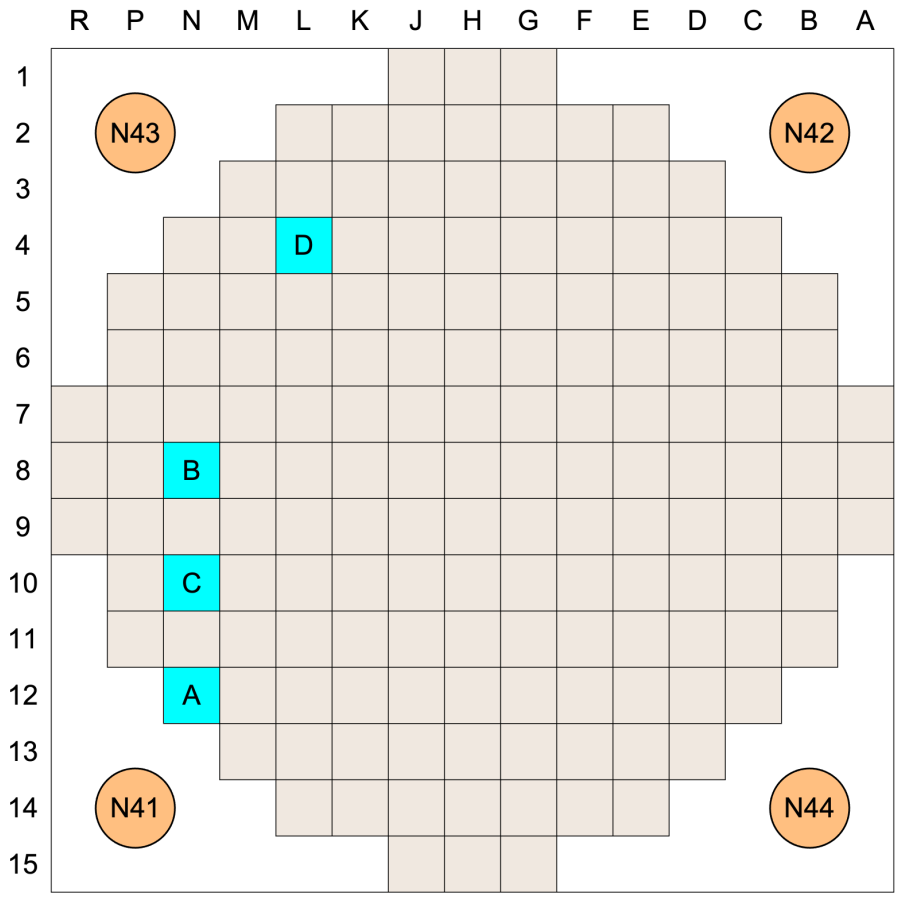

Figure 2.1: The radial positions of the four in-core detectors.

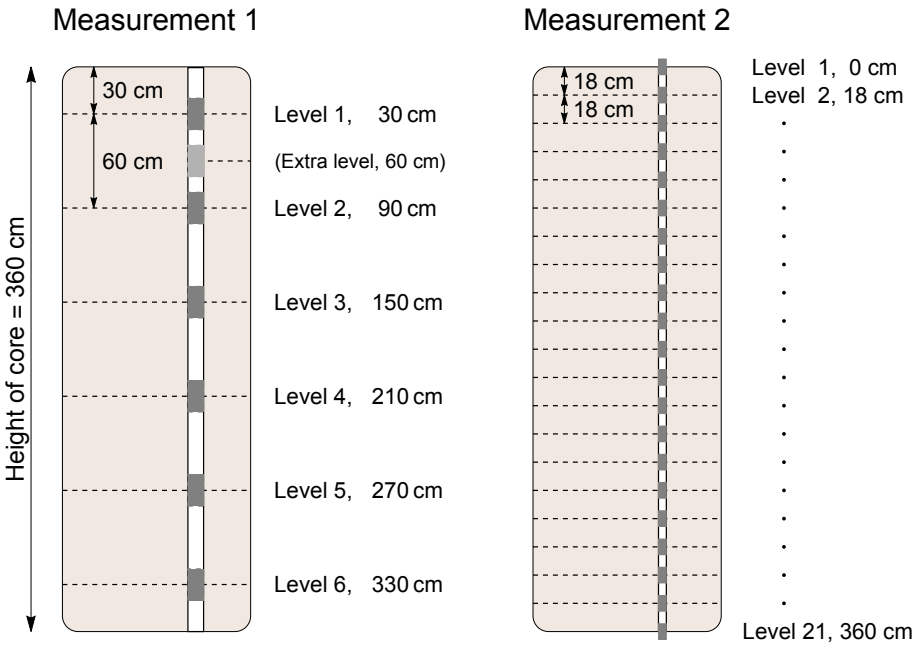

Figure 2.2: The axial positions of the measurement points in the two measurements.

referred to as Measurement 1 and Measurement 2, respectively. In Measurement 1, data were recorded at 6 axial levels (in Stage 2021 and extra 7th level was added), each measurement being 20 minutes long in 2020 and 30 minutes long in 2021. In 2020, the measurement was taken in one sequence, and the data from the six different levels were stored in one single file. In 2021, the data from the different levels were stored in different files, which alleviates the data handling at the analysis.

Table 2.2: The measurement data structure of the two in-core measurements in Ringhals 3 on 2020-12-01

Channel	Measurement point
0	Time
1	N41U DC
2	N42U DC
3	N43U DC
4	N44U DC
5	N41L DC
6	N42L DC
7	N43L DC
8	N44L DC
9	N41U AC
10	N42U AC
11	N43U AC
12	N44U AC
13	IncoreA_N12 AC
14	IncoreB_N08 AC
15	IncoreC_N10 AC
16	IncoreD_L04 AC

Table 2.3: The measurement data structure of the two in-core measurements in Ringhals 3 on 2022-04-08

Channel	Measurement point
0	Time
1	N41U DC
2	N42U DC
3	N43U DC
4	N44U DC
5	IncoreA_N12 AC
6	IncoreB_N08 AC
7	IncoreC_N10 AC
8	IncoreD_L04 AC
9	N41U AC
10	N42U AC
11	N43U AC
12	N44U AC
13	N41L AC
14	N42L AC
15	N43L AC
16	N44L AC

In Measurement 2, data were taken at 21 axial positions, with a one-minute measurement at each axial level. The measurement was taken in one sequence, without interrupting the data logging. The axial detector positions for Measurement 1 and 2 are shown in Fig. 2.2, indicating also the extra position in Measurement 1 in Stage 2021.

For the purposes of the present analysis, only Measurement 1 is relevant. Mea-

surement 2, which was made for the continuous wavelet transform method, was evaluated in Stage 2021 with simple CW transform. For comparison, those results will be also included after the results of the wavelet filtering and coherence methods.

It can be noted that in the reports of the two Stages, different notations were used for the axial positions and their quantitative values. In this report we will use those of Stage 2021, such that the quantitative value of the positions of the measurement levels in centimetres follows now the Ringhals convention, i.e. the distances are now measured from the top of the core.

Regarding the measurement system, a Westinghouse digital Flux Mapping System was installed in R3 during the outage 2016. The thermal neutron sensitivity of the four in-core flux detectors (fission chambers) ranges up to 10^{14} nv, although noticeable variation of the sensitivity amongst the detectors can be observed. The sampling frequency was 62.5 Hz for all three sets of measurements.

The structure of the data logging was similar to that of the ex-core measurements, in that four in-core detector AC signals replaced four of the regular ex-core DC signals. The data structure was slightly different between the two Stages what regards which channels were used for which detector. The data structure, i.e. the registered quantities (static and fluctuating parts, i.e. DC and AC, respectively) are shown in Table 2.2 for the measurements in Stage 2020, made on 2020-12-01, and in Table 2.3 for the measurements in Stage 2021, made on 2022-04-08 December 2020.

From Tables 2.2 and 2.3 it is seen that for the in-core detectors, the DC component was not registered. This means that, unlike with the ex-core measurements, there is no possibility to normalise the signals to their static (average) value. This does not incur much problem for the investigations of the thimble tube vibrations, as long as one is interested in the structure of the spectra and the coherences/phases, without trying to perform a quantitative trend analysis.

2.4 Results of the analysis of the measurements from Stage 2020

Measurement 1 from Stage 2020 was evaluated by wavelet filtering and wavelet coherence methods. In that Stage, Measurement 1 was executed in one sequence, i.e. the results for all levels are contained in one single file. This is how the data were recorded in all previous in-core measurement, such as in Stage 12. This means that the data series corresponding to the different levels have to be extracted manually, by inspecting the spikes in the time signal, indicating the movement of the detector from a given level to the next one. In this process, due to the data logging during the moving of the detectors, a certain amount of data inevitably has to be deleted.

2.4.1 Wavelet filtering

The results are shown in Figs. 2.3 - 2.8 for axial levels 1 to 6. In each figure the results from both the Meyer (left column) and Haar (right column) wavelets are shown.

It is seen that the results are slightly different between the different levels, as well as that they differ between the Meyer and the Haar wavelets. A general trend

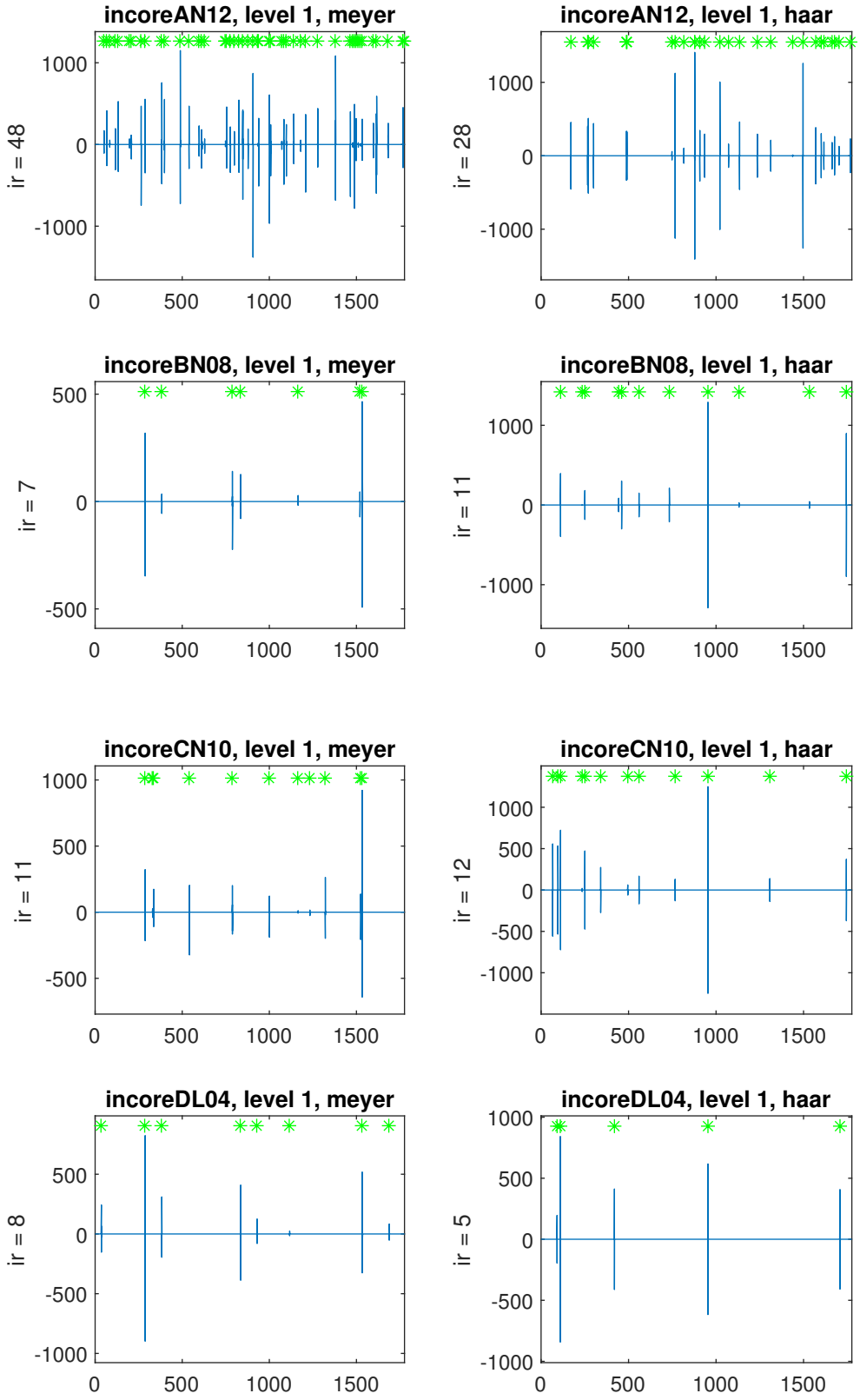

Figure 2.3: The results of the wavelet filtering of the measurement in 2020, level 1

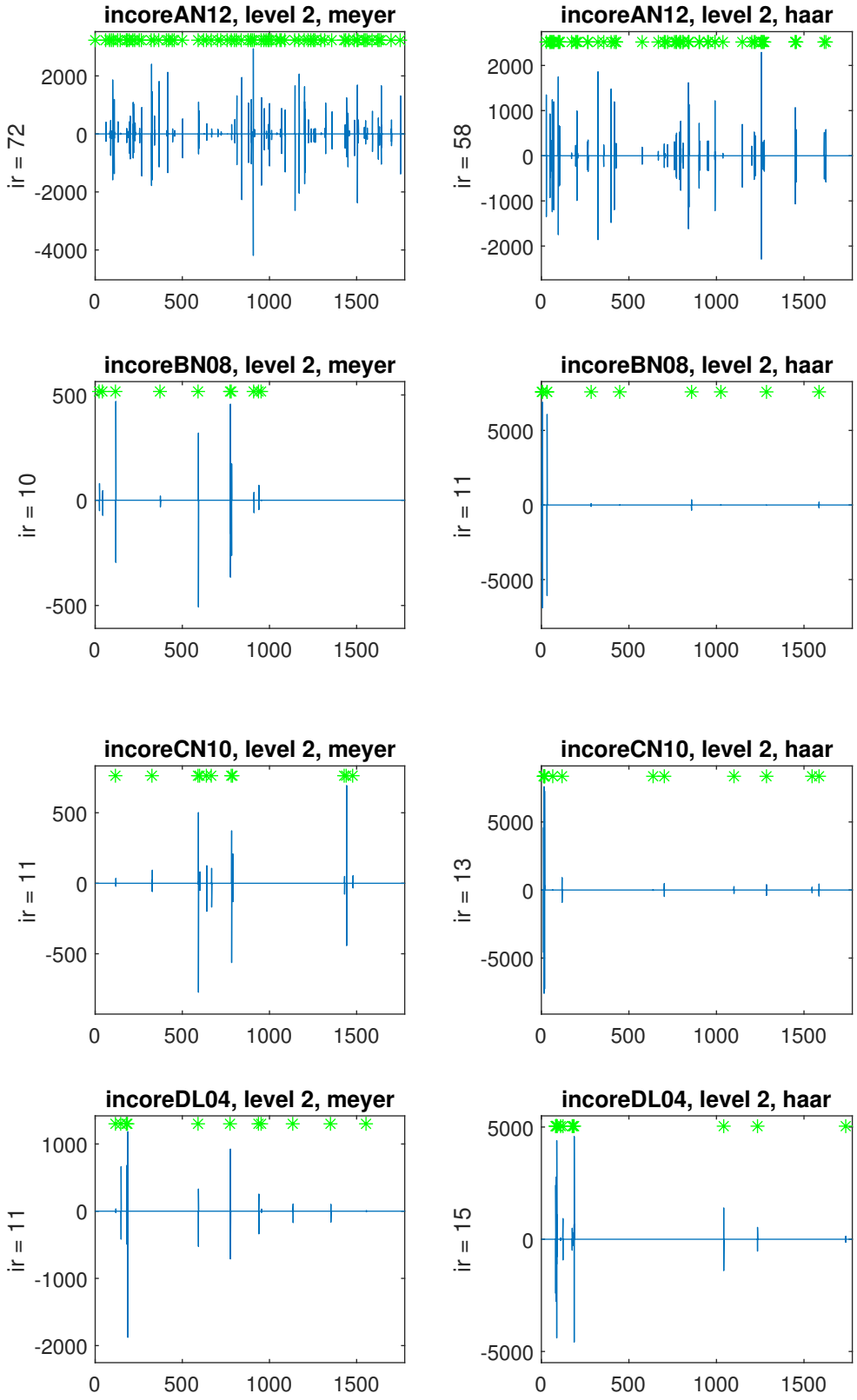

Figure 2.4: The results of the wavelet filtering of the measurement in 2020, level2

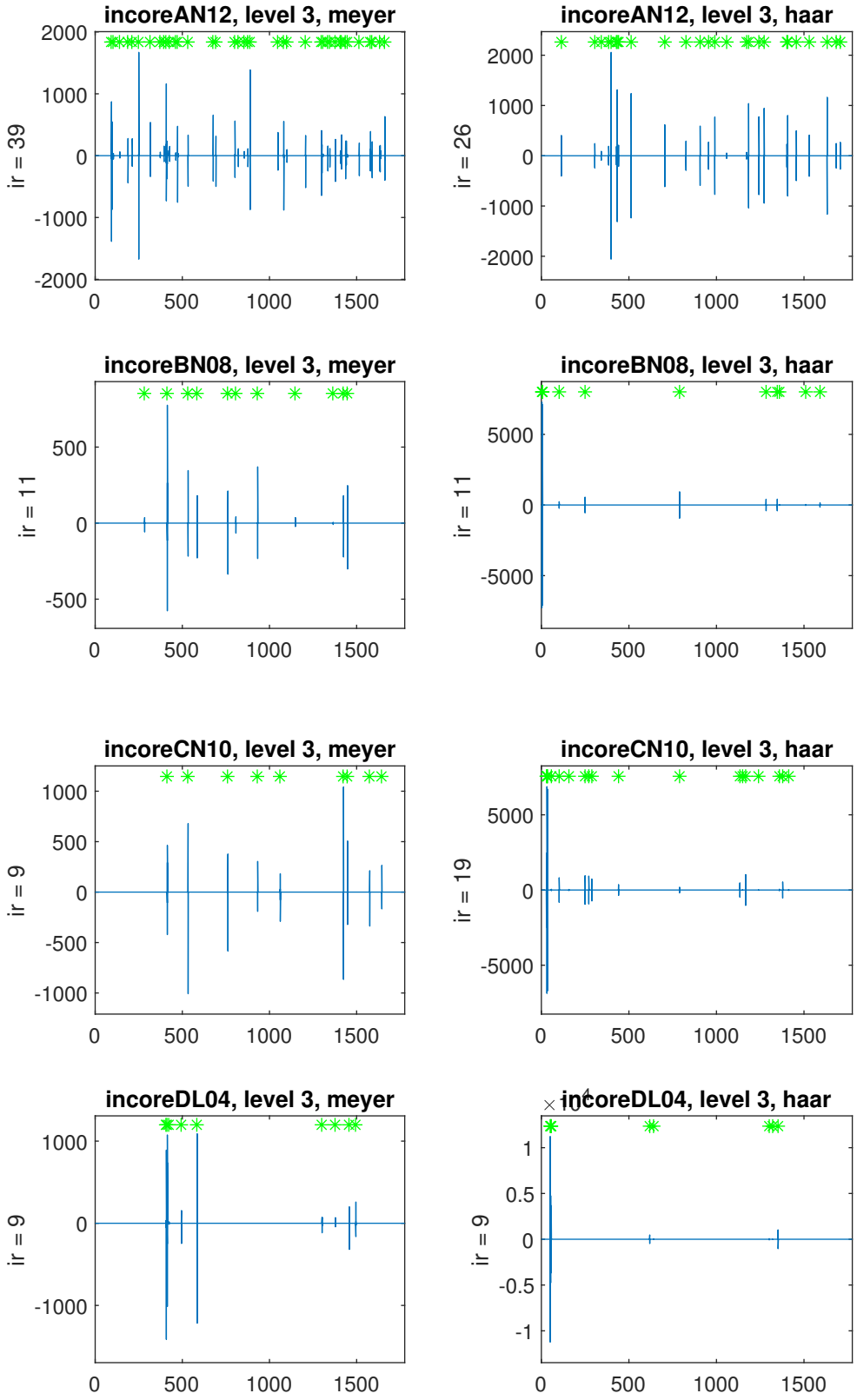

Figure 2.5: The results of the wavelet filtering of the measurement in 2020, level 3

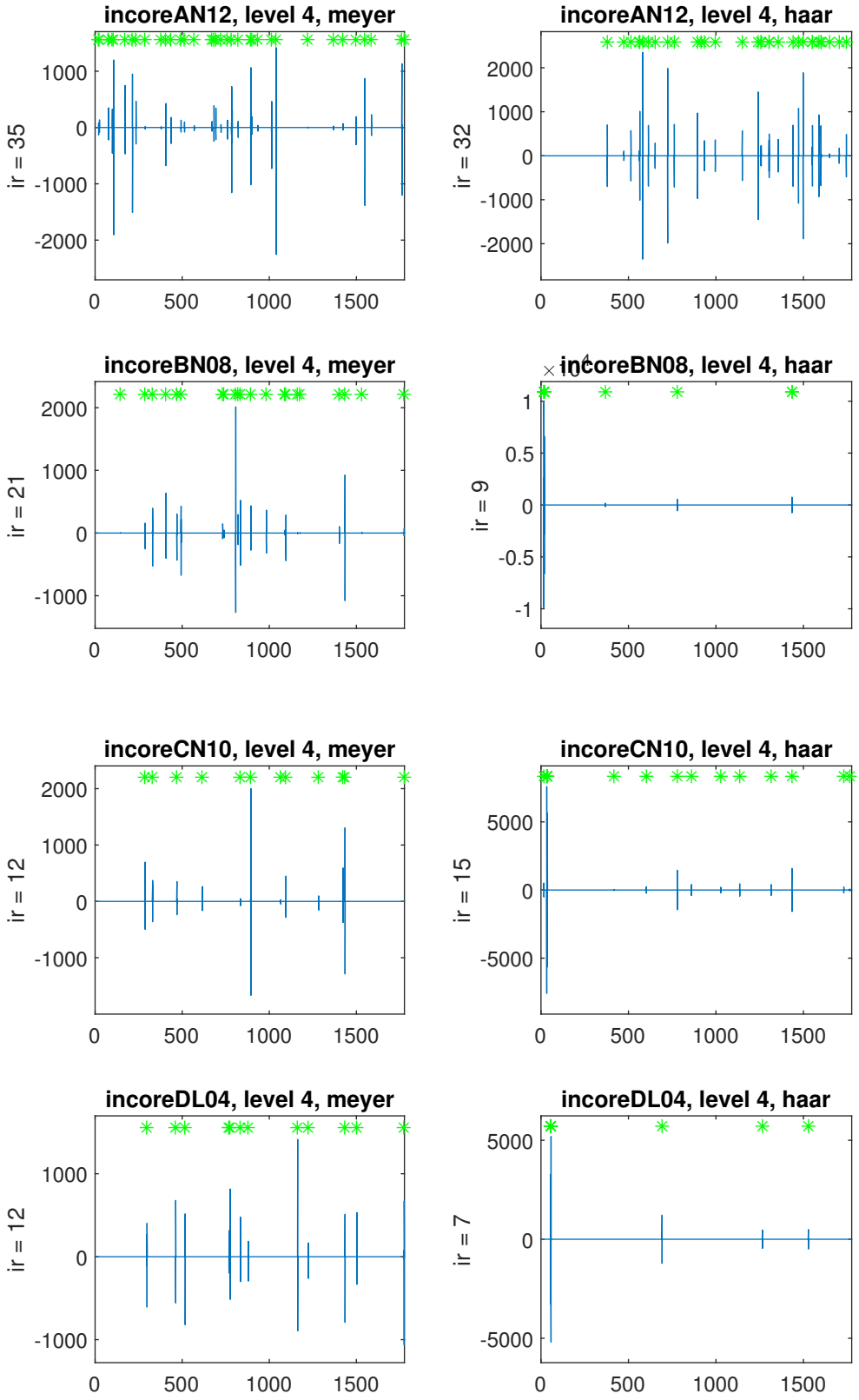

Figure 2.6: The results of the wavelet filtering of the measurement in 2020, level 4

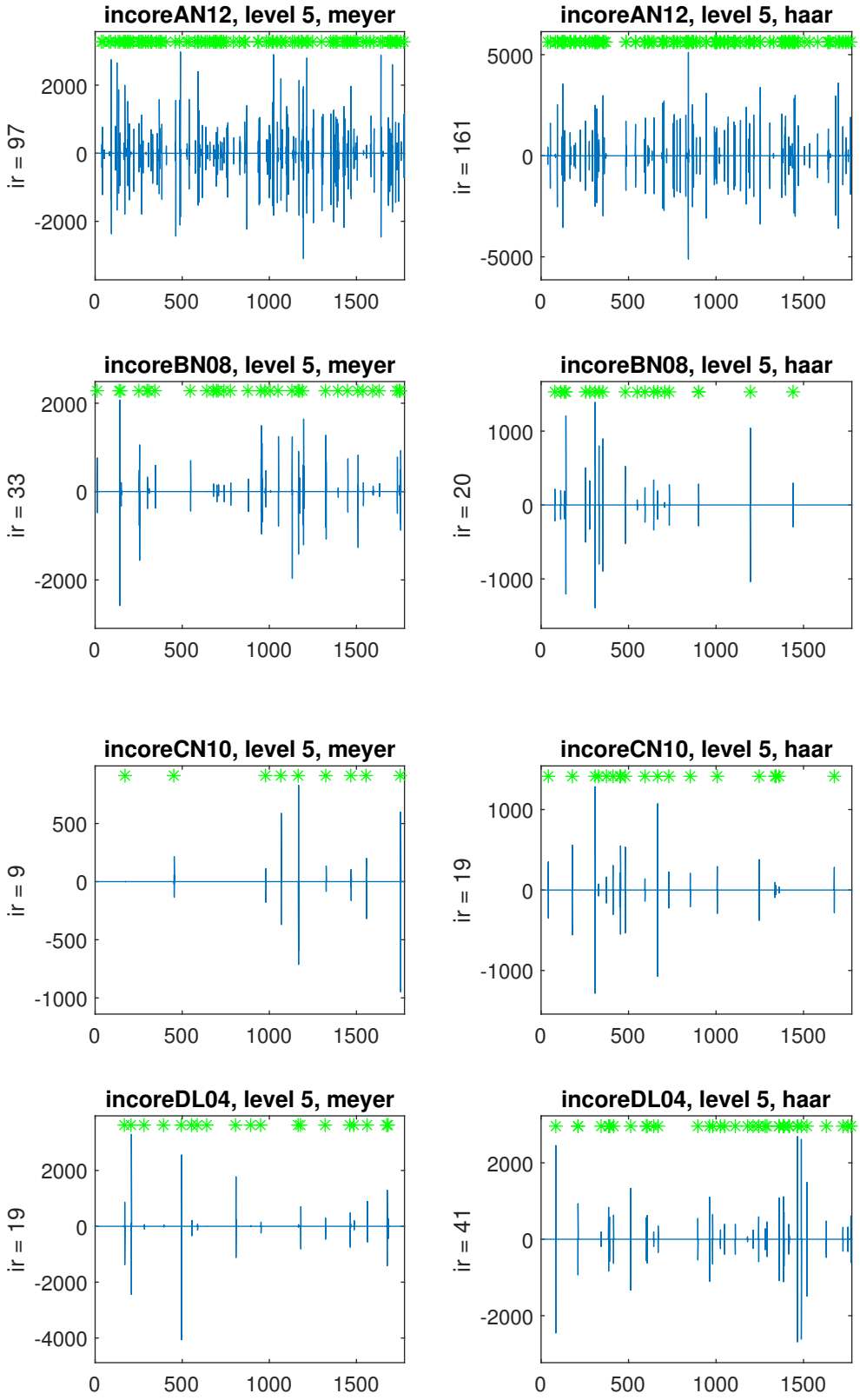

Figure 2.7: The results of the wavelet filtering of the measurement in 2020, level 5

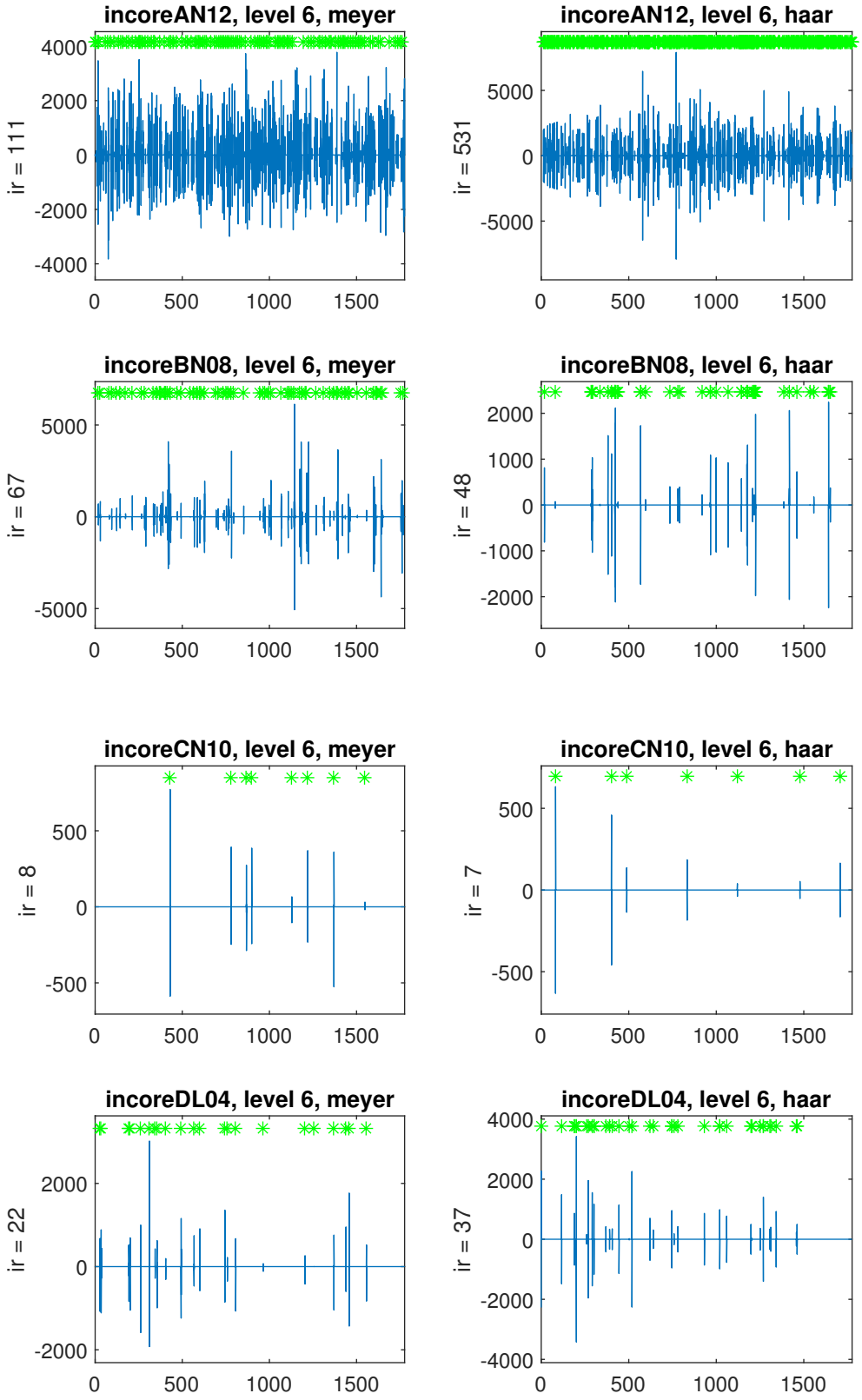

Figure 2.8: The results of the wavelet filtering of the measurement in 2020, level 6

is that the impact rates (IRs) are higher at the lower levels. The IR is the highest at level 6, i.e. the lowermost level (see Fig. 2.2). It is somewhat difficult to get a good overview due to the scattering of the results between the different levels and between the Meyer and the Haar wavelets. One definite fact is that detector A (at N12) is designated as having the highest IR at all levels and by both wavelets. For the rest of the detectors, one can summarize the results for the 6 levels and the two wavelets by assigning a value between 1 and 4 for each detector at each level and each wavelet, such that the detector with the highest IR has 4 and the one with the lowest IR getting 1, and then taking a sum of all levels and wavelets. This gives by far the highest ranking to detector A, second highest to B, whereas C and D end up with the same ranking. Taking only the results from the Meyer wavelets results in the ranking A (highest), B, D and C (lowest). One gets also the same sequence if taking only the results from level 6, where the IR is the highest for all levels.

This ranking is actually in a very good agreement with the more intuitive judgement, made on the same detectors in Stage 2021 (which was though made on a later measurement): Detector A (N12) was judged to have the largest probability of impacting, then detectors B (N08) and D (L04). Detector C (N10) had the least probability of impacting. The wavelet filtering results yield a very similar result.

2.4.2 Wavelet coherence

The wavelet coherences were calculated only for the closest pairs of detectors, i.e. between A-C, C-B and B-D. The coherences for levels 1 - 6, shown in separate figures for the Meyer and the Haar wavelets, respectively, are shown in Figs 2.9 - 2.20.

As mentioned previously, the application of the wavelet coherence technique is not as straightforward for the thimble tube vibrations and impacting as for the BWR case. In the latter, the coherence is taken between two detectors in the same detector tube, and the coherence unambiguously refers to the given detector string. What regards the thimble tube vibrations, the coherence is taken between two detectors in different strings, i.e. between two detectors at different radial locations. Hence the result can indicate impacting in either of the two thimble tubes, or a thimble tube in between the two detectors.

A further circumstance, which makes the interpretation of the wavelet filtering results difficult, is that in contrast to the case of instrument tube vibrations, the frequency of the possible thimble tube vibrations is not known. Apart from some singular cases, such as detector A at level 1 (30 cm from the core top) in Stage 2021, hardly any visible tops are seen in the power spectra of the in-core detectors below 8 Hz (the beam mode frequency).

Accordingly, the results in Figs 2.9 - 2.20 do not lend themselves for drawing definite conclusions. A general feature of both wavelets is that they show lower coherences for the lower levels than for the higher ones. This is in contrast to the wavelet filtering results, where higher impact rates were found at level 6.

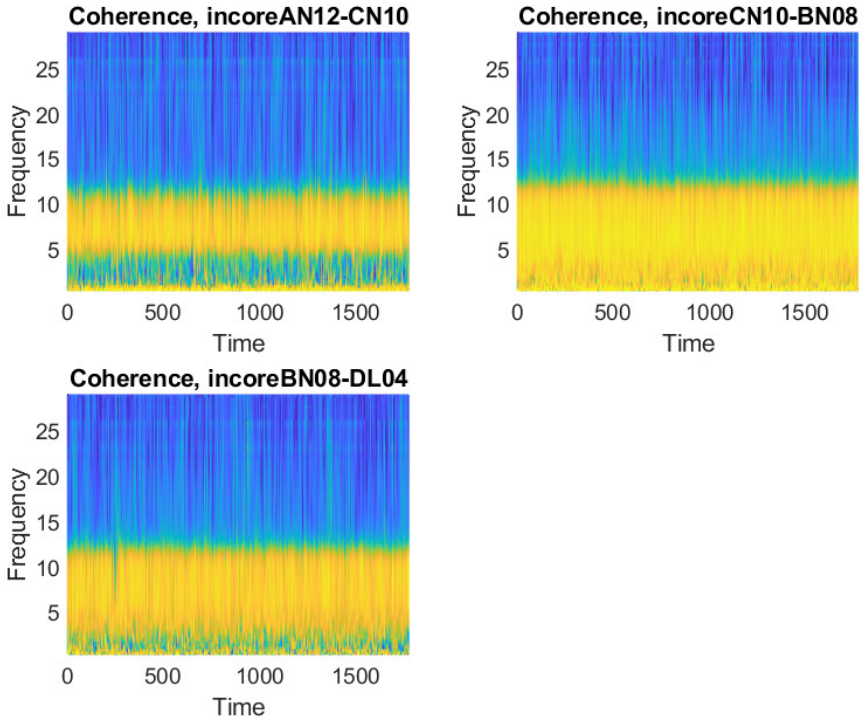

Figure 2.9: The result of the wavelet coherence of the measurement in Stage 2020, level 1, Meyer wavelets

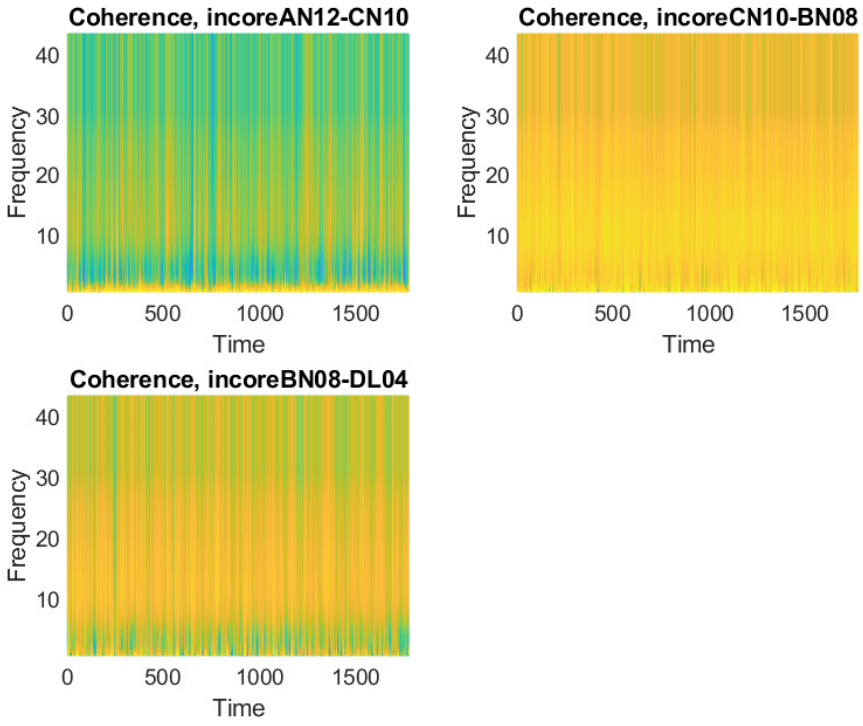

Figure 2.10: The result of the wavelet coherence of the measurement in Stage 2020, level 1, Haar wavelets

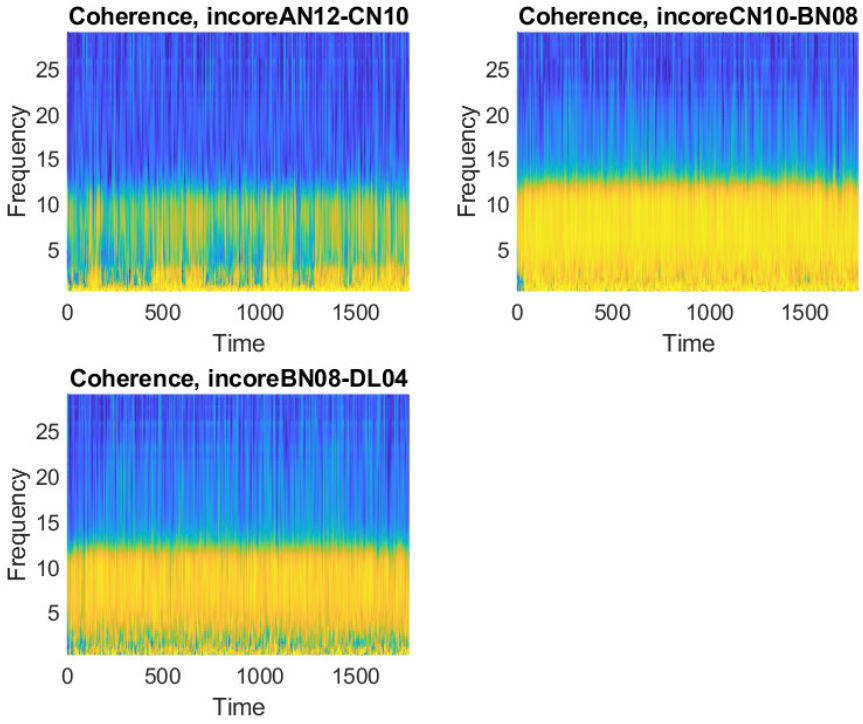

Figure 2.11: The result of the wavelet coherence of the measurement in Stage 2020, level 2, Meyer wavelets

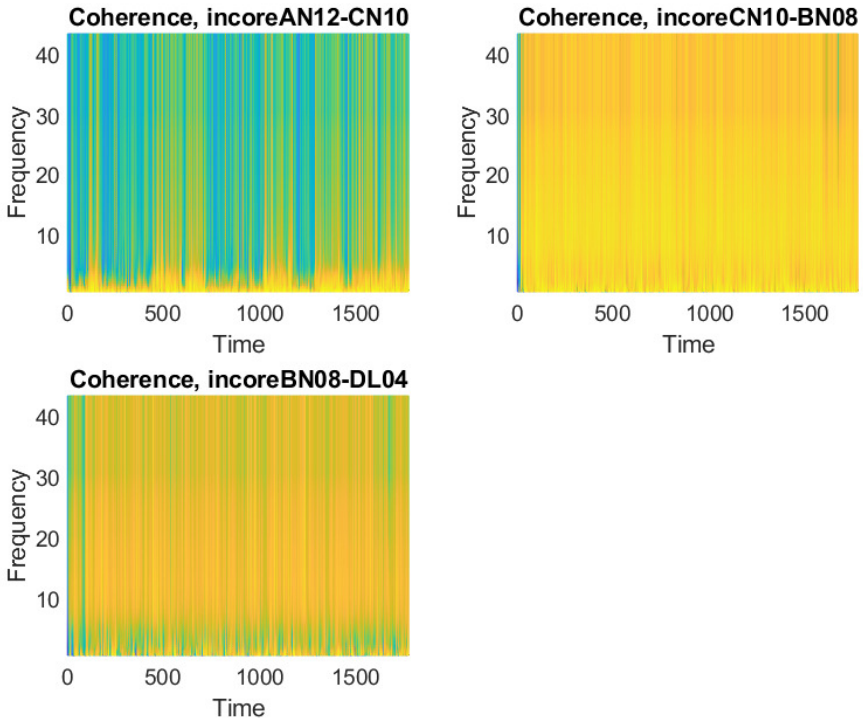

Figure 2.12: The result of the wavelet coherence of the measurement in Stage 2020, level 2, Haar wavelets

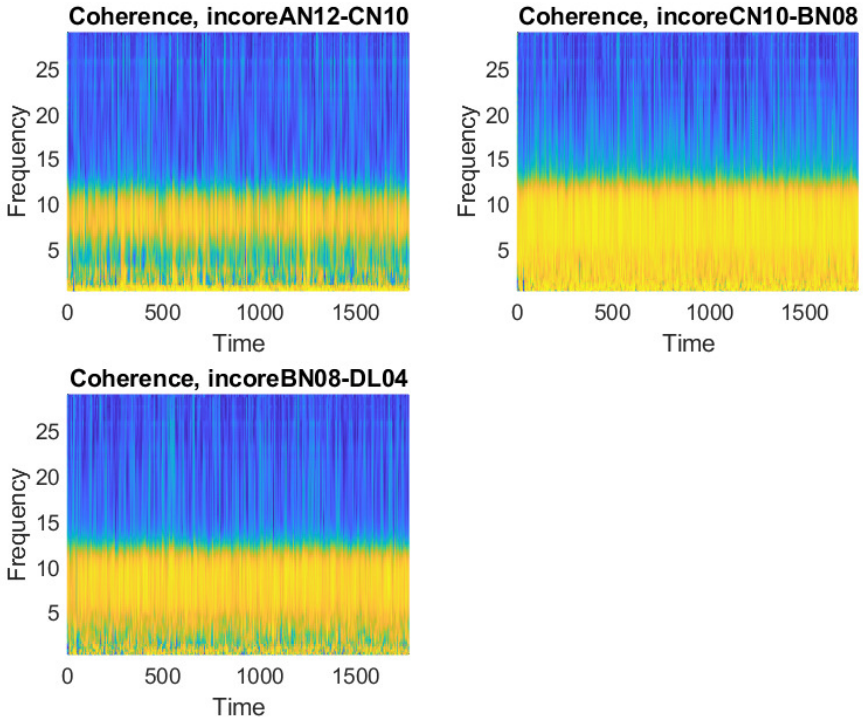

Figure 2.13: The result of the wavelet coherence of the measurement in Stage 2020, level 3, Meyer wavelets

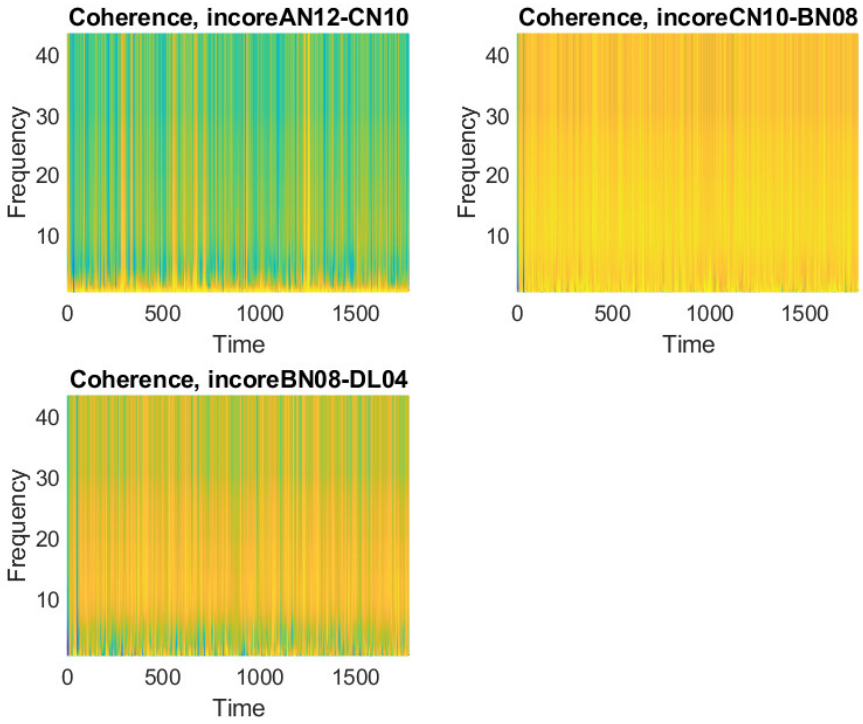

Figure 2.14: The result of the wavelet coherence of the measurement in Stage 2020, level 3, Haar wavelets

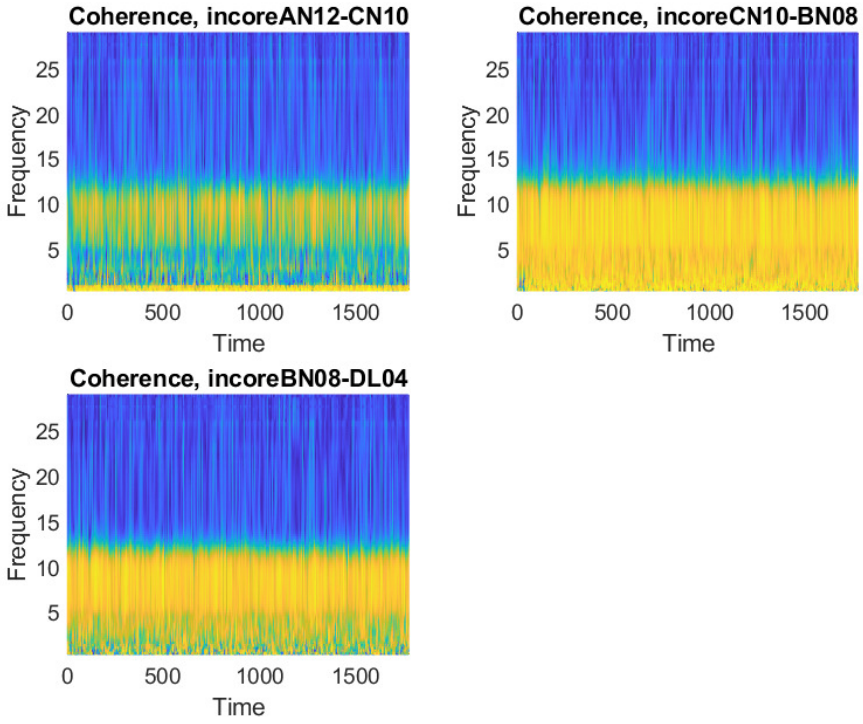

Figure 2.15: The result of the wavelet coherence of the measurement in Stage 2020, level 4, Meyer wavelets

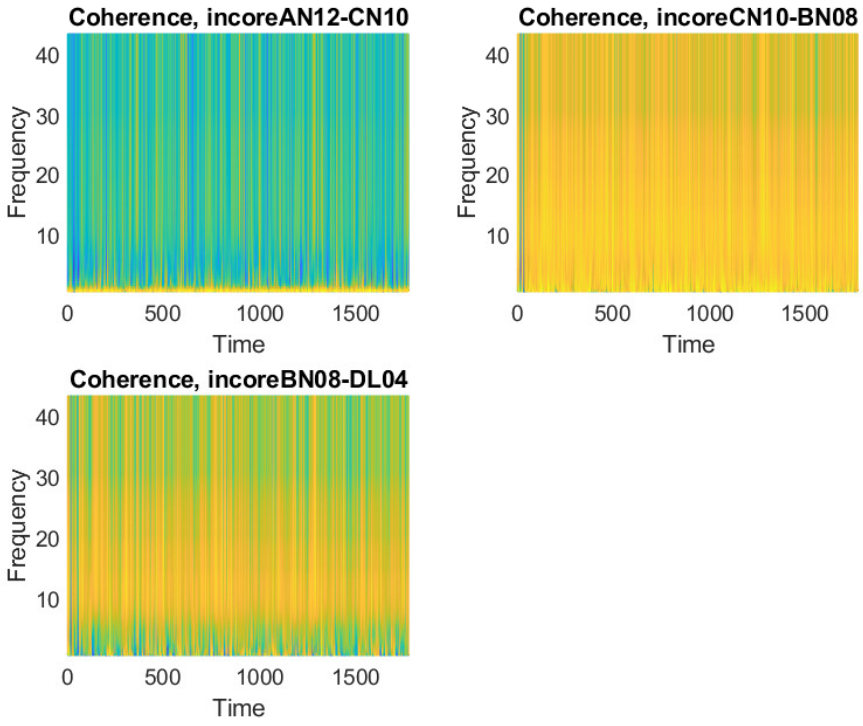

Figure 2.16: The result of the wavelet coherence of the measurement in Stage 2020, level 4, Haar wavelets

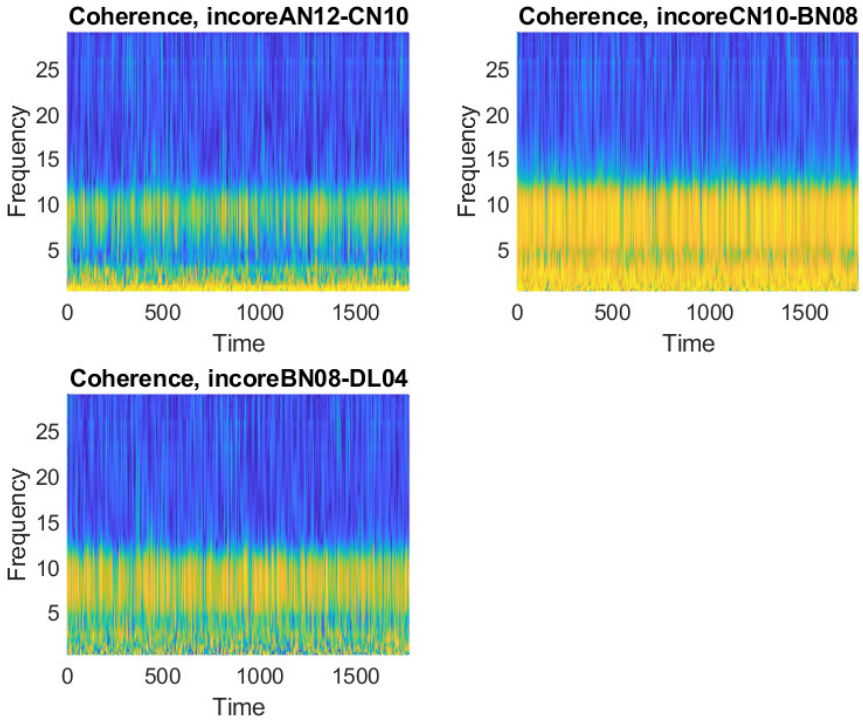

Figure 2.17: The result of the wavelet coherence of the measurement in Stage 2020, level 5, Meyer wavelets

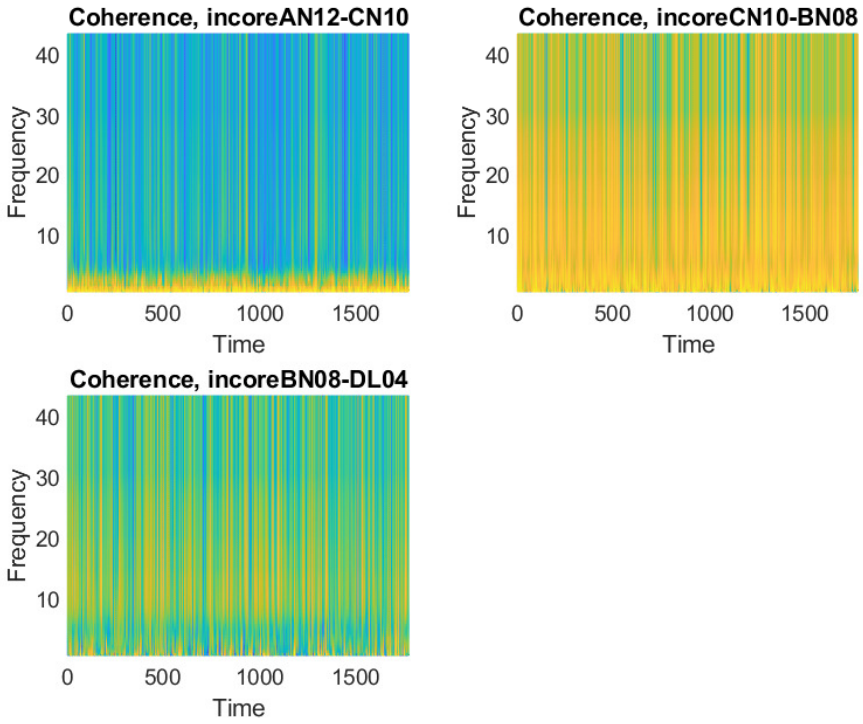

Figure 2.18: The result of the wavelet coherence of the measurement in Stage 2020, level 5, Haar wavelets

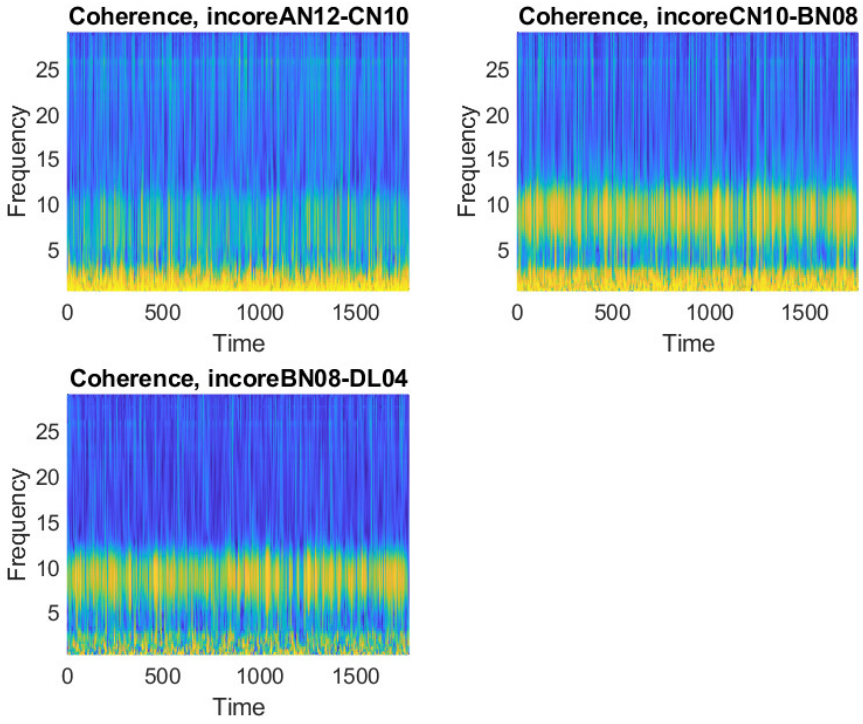

Figure 2.19: The result of the wavelet coherence of the measurement in 2020, level 6, Meyer wavelets

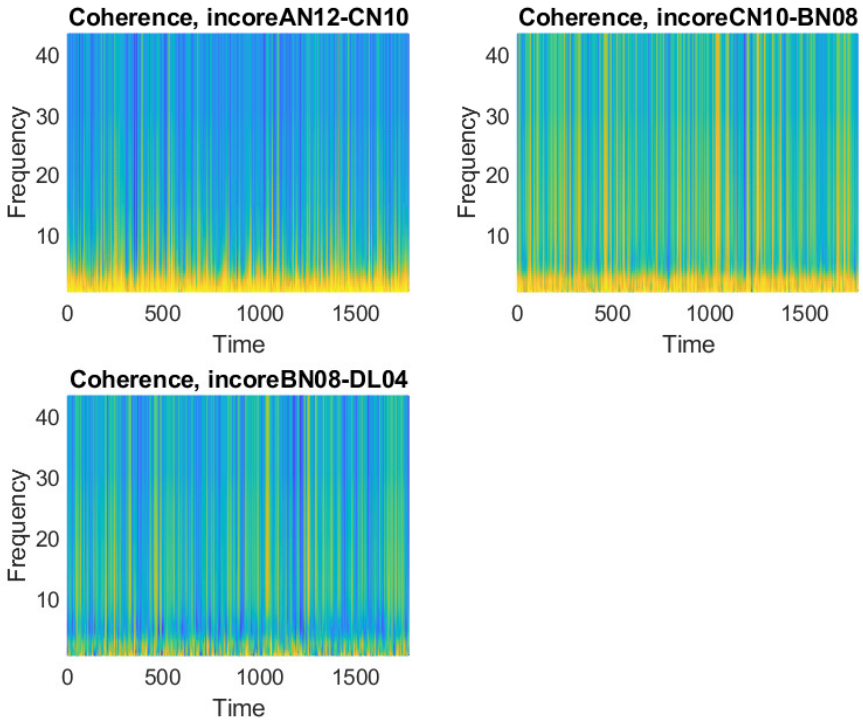

Figure 2.20: The result of the wavelet coherence of the measurement in 2020, level 6, Haar wavelets

Out of the two different wavelets, the coherences by the Haar wavelet, although seemingly showing relatively high coherences for at least two pairs at most levels, do not show any structure which could be interpreted. The results for the Meyer wavelet are more suitable for some interpretation. They are more resembling to the coherences which were seen in the wavelet coherences in the BWR analysis, reported in e.g. Stage 12 [10], in that there are stripes of high coherence in the frequency range 5-10 Hz. By physical intuition one might expect that the same frequency range could be relevant also for the case of vibration and impacting of thimble tubes. In this frequency range, the coherences are highest for the pair C-B, followed by B-D and finally for A-C. This ranking is the same for all levels although, in contrast to the IR parameter, the coherences are higher at the higher levels.

Another deviation between the IR and the wavelet coherence results is the internal ranking regarding the severity, since the IR method pointed out detector A as the one with the highest impact rate, whereas the coherences are higher for the pair C-B. This apparent contradiction can arise from the fact that, as mentioned earlier, the wavelet coherence can concern either of the detectors in the pair, or a thimble tube in a third, close position, most likely in between the two detectors. In this sense the high coherence between detectors C and B may indicate a thimble tube vibration in position N11.

2.5 Evaluation of the Measurements in Stage 2021

2.5.1 Wavelet filtering

The results of the wavelet filtering are shown in the same sequence as for Stage 2020, i.e. starting with the uppermost level, and progressing to the lower levels, ending with the lowermost one. However, as mentioned earlier and as is indicated in Fig. 2.2, in these measurements, made on 2022-03-30, in Measurement 1 an extra level at 60 cm was also included. This measurement was also evaluated, and to keep the sequential numbering, it was called level 3. This way the position at 90 cm, which in the previous Stage was called level 2, here became level 3, and so on. The results for the seven axial levels are shown in Figs 2.21 - 2.26, with both the application of Meyer (left column) and Haar (right column) wavelets.

These results are somewhat less unambiguous than for those in Stage 2020. In general, the IR values decreased as compared to those in 2020, and also the differences between the different levels are much smaller. In addition, the order of severity is reversed in the sense that the highest IR values are found at the the two uppermost levels (level 1 and 2).

The best way to condense the results is to perform the same type of ranking as with the results of Stage 2020, namely assigning the values 1 - 4 to each detector and level according to the order of the IR numbers, and summarising for all levels and the two wavelets. This procedure leads with unambiguously to the same ranking as for the previous stage, i.e. A (highest severity), B, D, and C (lowest severity). This is in good agreement with the ranking of the measurements from 2020.

More investigations would be necessary to understand the reason for the differ-

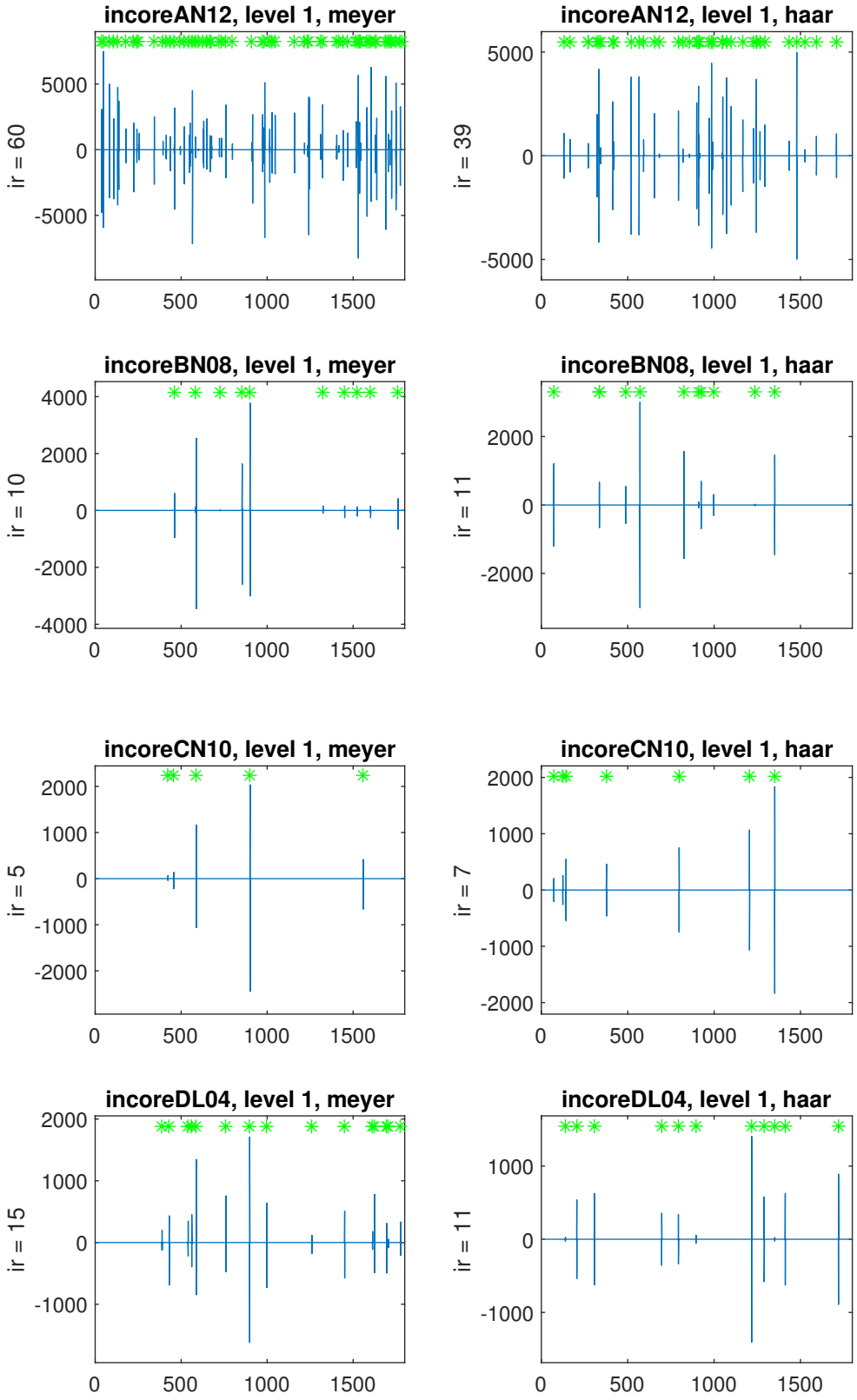

Figure 2.21: The results of the wavelet filtering of the measurement in 2021, level 1

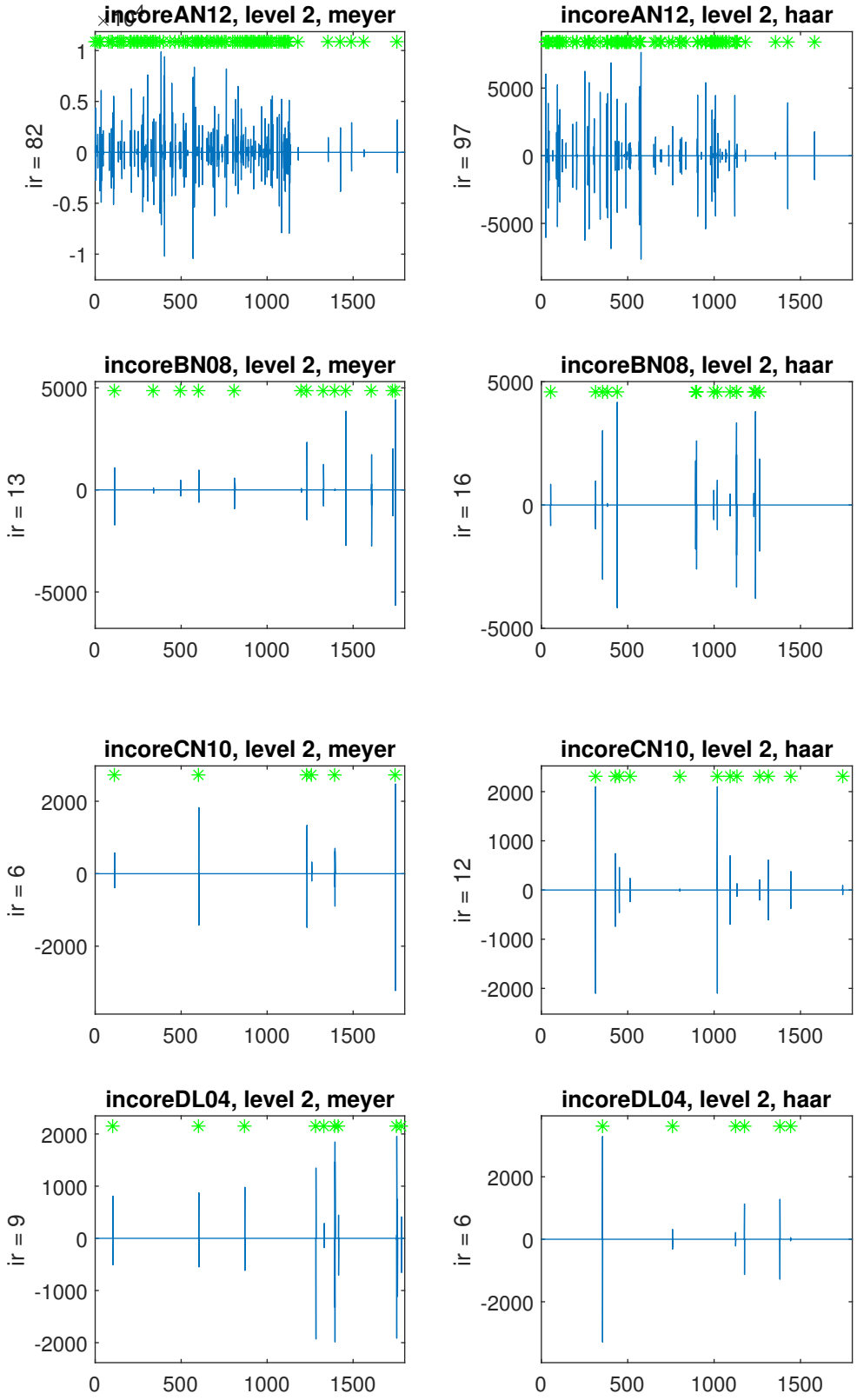

Figure 2.22: The results of the wavelet filtering of the measurement in 2021, level 2

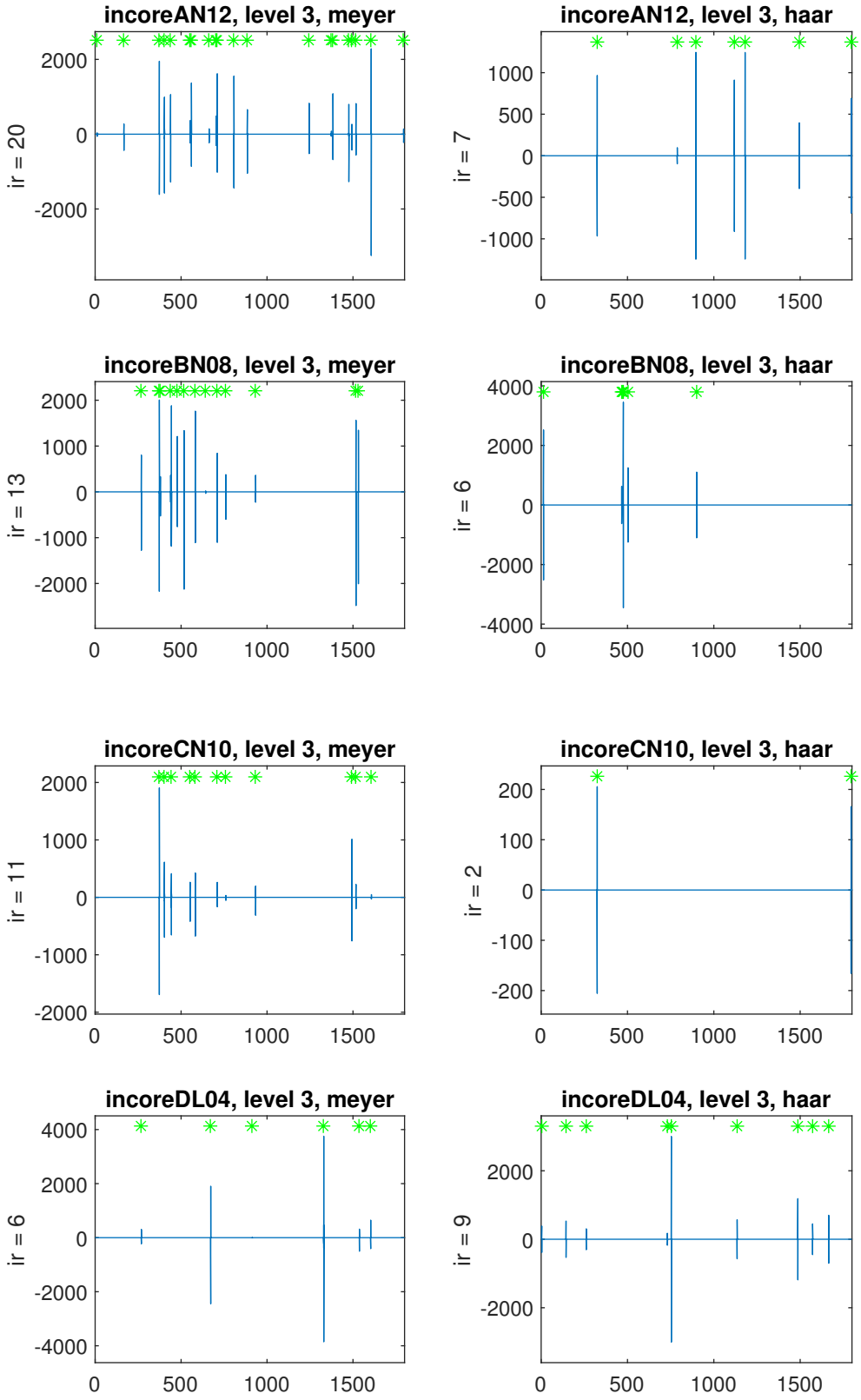

Figure 2.23: The result of the wavelet filtering of the measurement in 2021, level 3

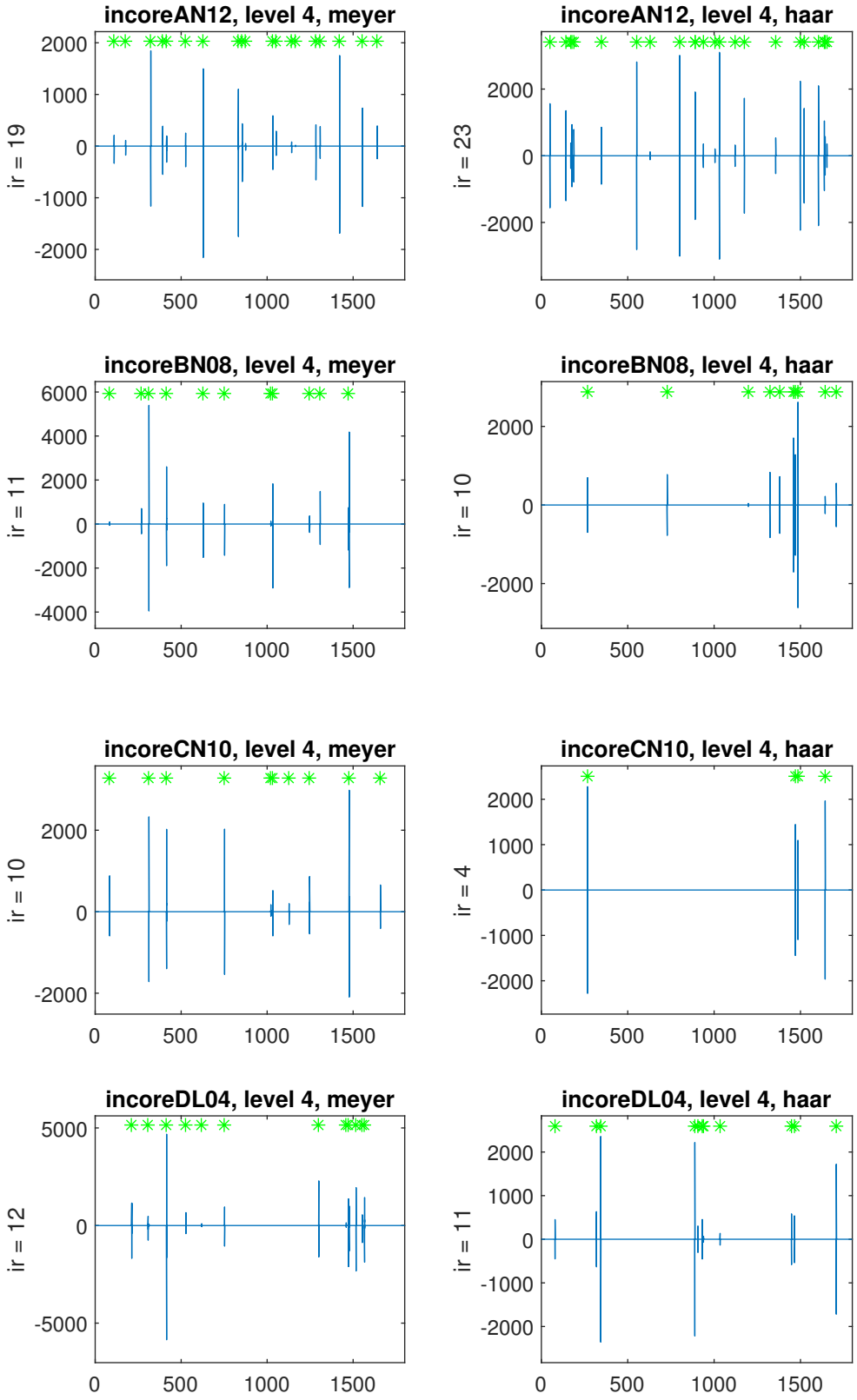

Figure 2.24: The result of the wavelet filtering of the measurement in 2021, level 4

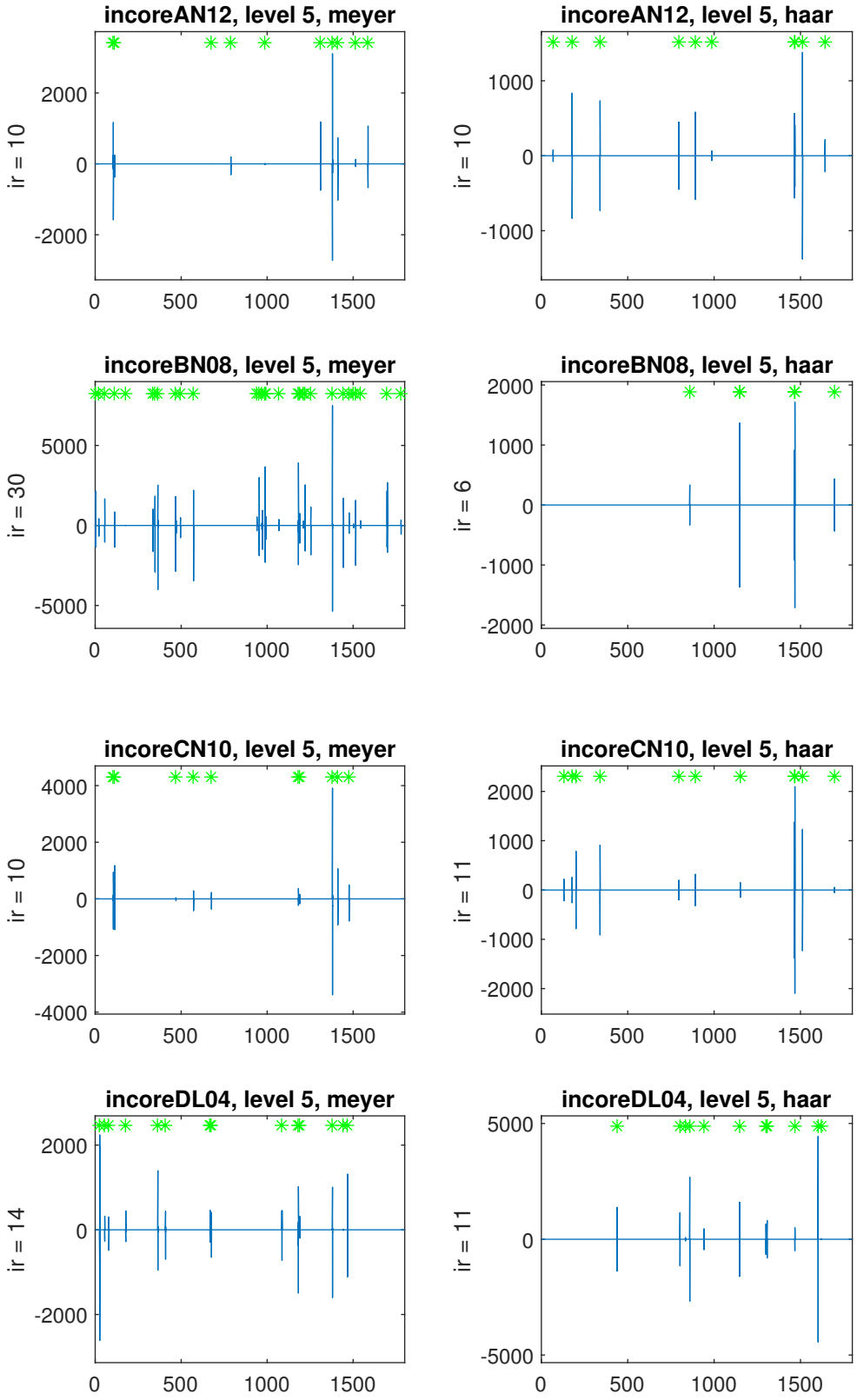

Figure 2.25: The result of the wavelet filtering of the measurement in 2021, level 5

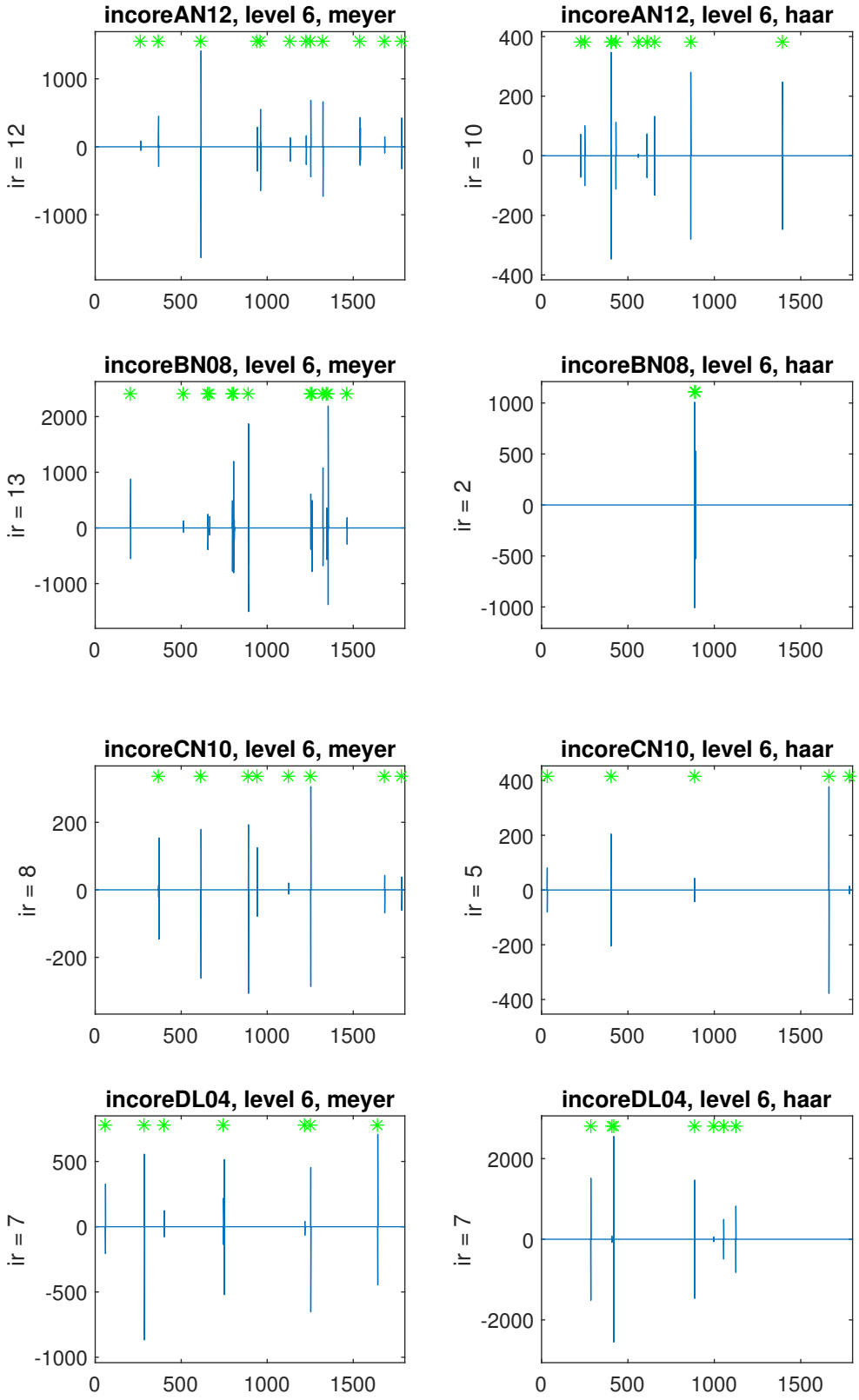

Figure 2.26: The result of the wavelet filtering of the measurement in 2021, level 6

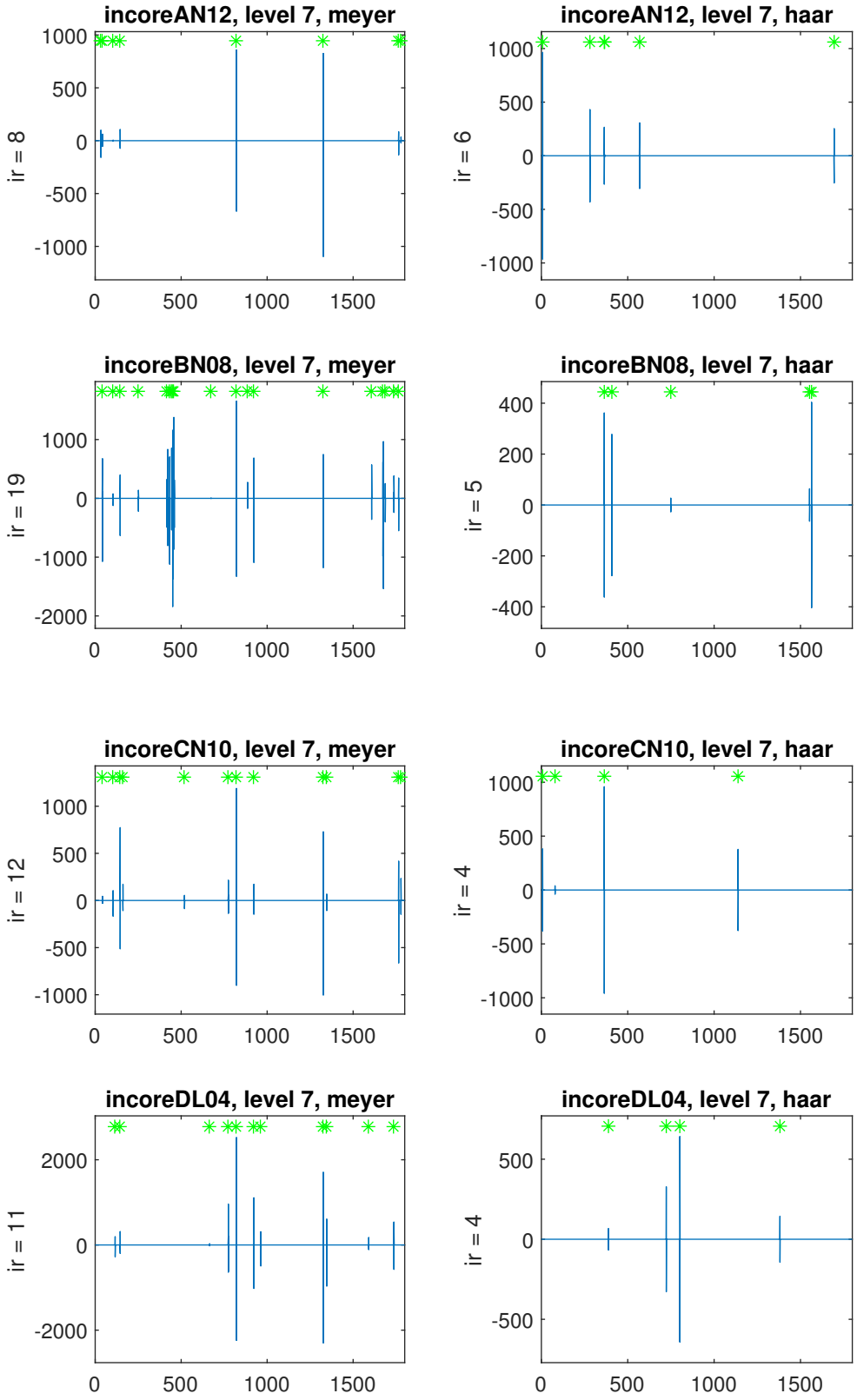

Figure 2.27: The result of the wavelet filtering of the measurement in 2021, level 7

ences between the 2020 and 2021 results. It is likely that the threshold used in the 2021 measurements was too high, leading to too low IR values. This leads to a high statistical uncertainty in the (low) IR values. A reliable ranking between the different thimble tube cases can only be made if the IR is sufficiently high, such as in the measurements in Stage 2020. This problem would be interesting to investigate further.

2.5.2 Wavelet coherence

The coherences for level 3 with Meyer wavelets are shown in Fig. 2.32 and the same with Haar wavelets in Fig. 2.33. The results for level 6 for the Meyer and the Haar wavelets are shown in Figs. 2.38 and 2.39, respectively.

These results show a somewhat better resemblance to the wavelet coherence results from Stage 2020 than the wavelet filtering results. The coherences calculated by the Haar wavelet still lack a structure which would be suitable for interpretation. The Meyer wavelet based coherences are similar, but not identical to those from 2020. They still show the characteristic stripes in the frequency band between 5 - 10 Hz, except between the pairs B - D at the higher levels. There are also some deviations, namely the coherences are larger now at the lower levels than on the higher, and between the three detector pairs, now the pairs A-C and C-B show the highest coherence. Out of these two, the pair C-B was pointed out also in the measurements in Stage 2020 as having the highest coherence.

In summarising, the attempt for reviving the wavelet filtering and wavelet coherence based detection and classification of thimble tube vibrations was promising in the sense that the analysis software was put into use. The results show the potentials of the method, and the results obtained are partially consistent between Stage 2020 and 2021. The IR parameter extracted by the wavelet filtering method has clearly a good potential to classify the severity of the impacting. The interpretation of the wavelet based coherence is less clear. More effort would be interesting to spend on both further analysis and improvement and optimisation of the method.

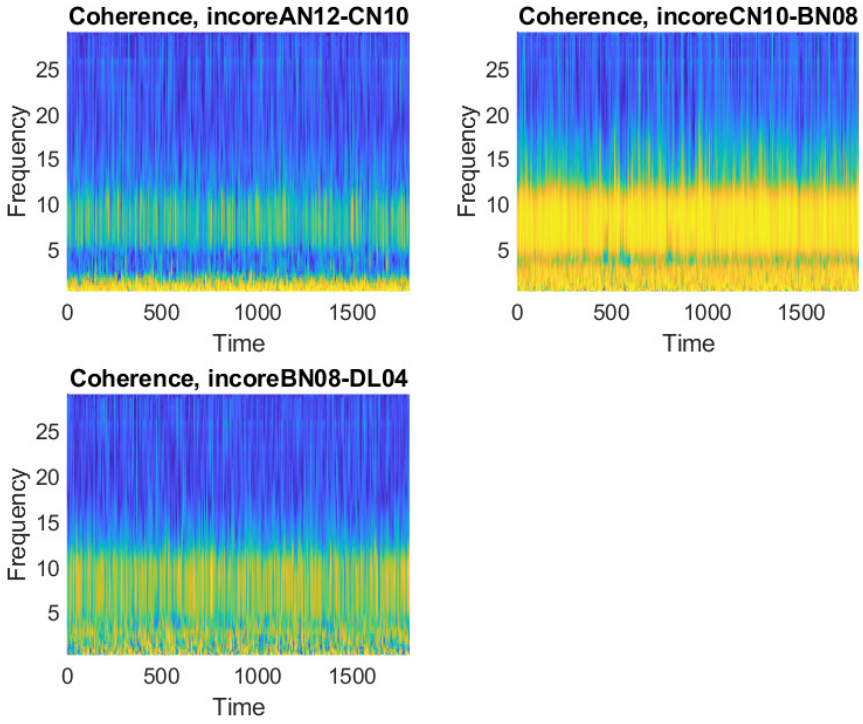

Figure 2.28: The results of the wavelet coherence of the measurement in Stage 2021, level 1, Meyer wavelets

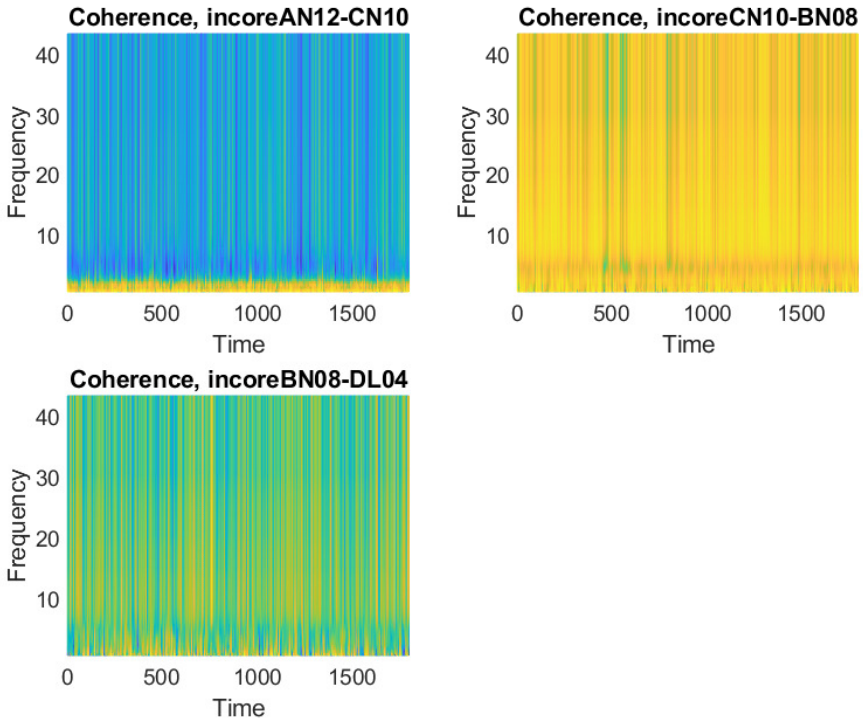

Figure 2.29: The results of the wavelet coherence of the measurement in Stage 2021, level 1, Haar wavelets

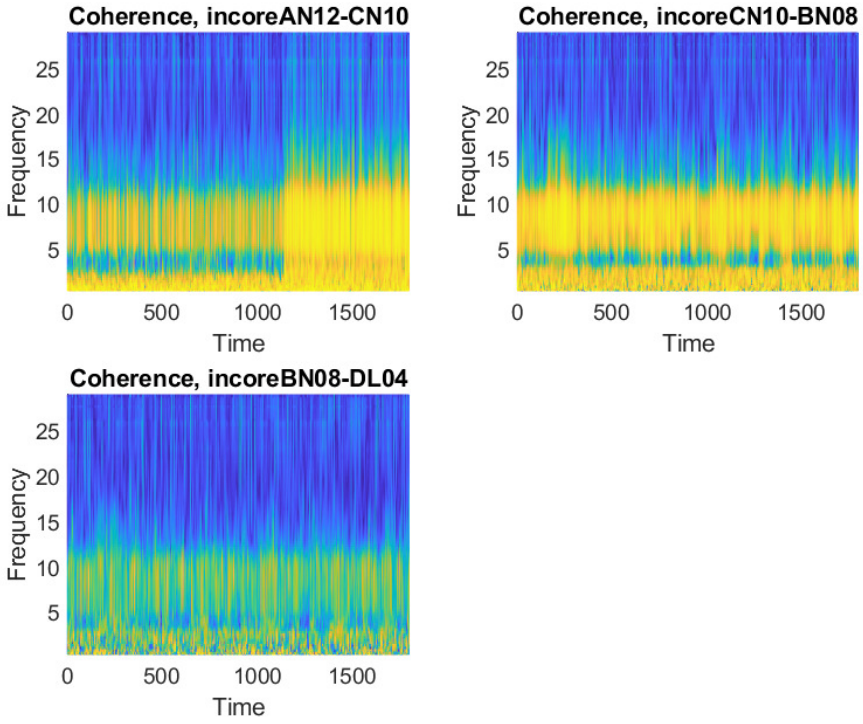

Figure 2.30: The result of the wavelet coherence of the measurement in Stage 2021, level 2, Meyer wavelets

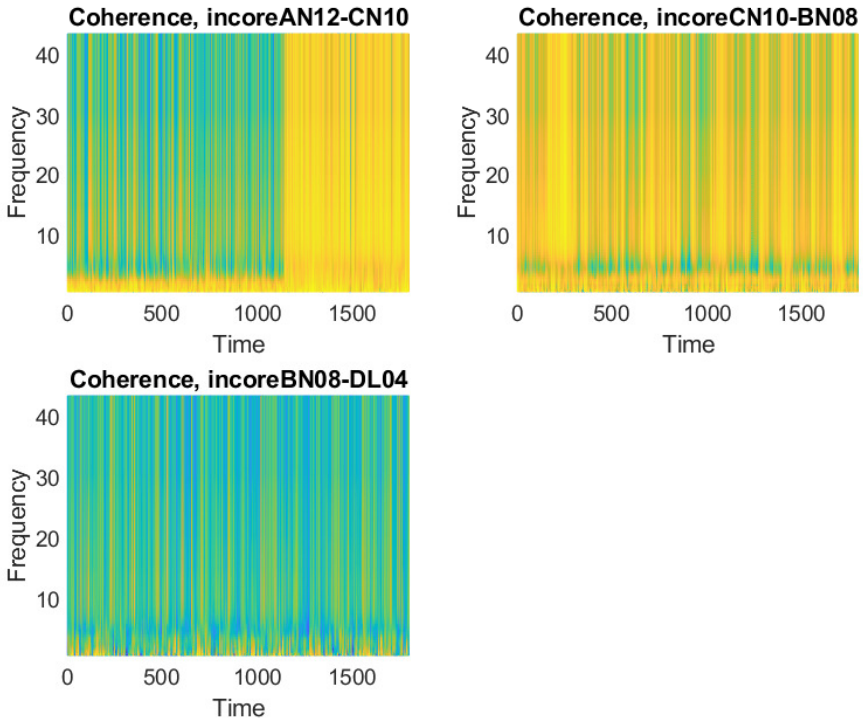

Figure 2.31: The result of the wavelet coherence of the measurement in Stage 2021, level 2, Haar wavelets

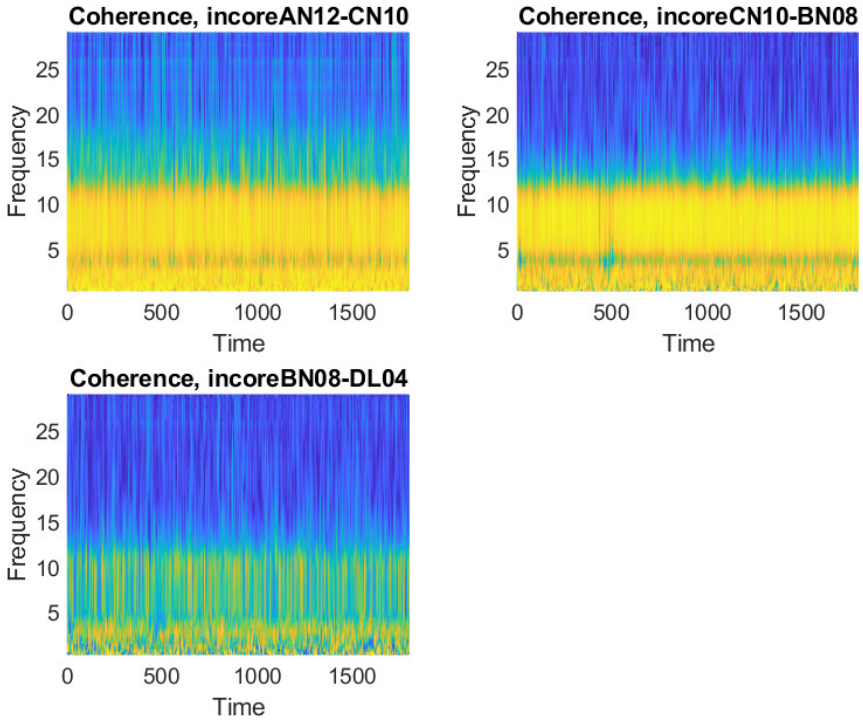

Figure 2.32: The result of the wavelet coherence of the measurement in Stage 2021, level 3, Meyer wavelets

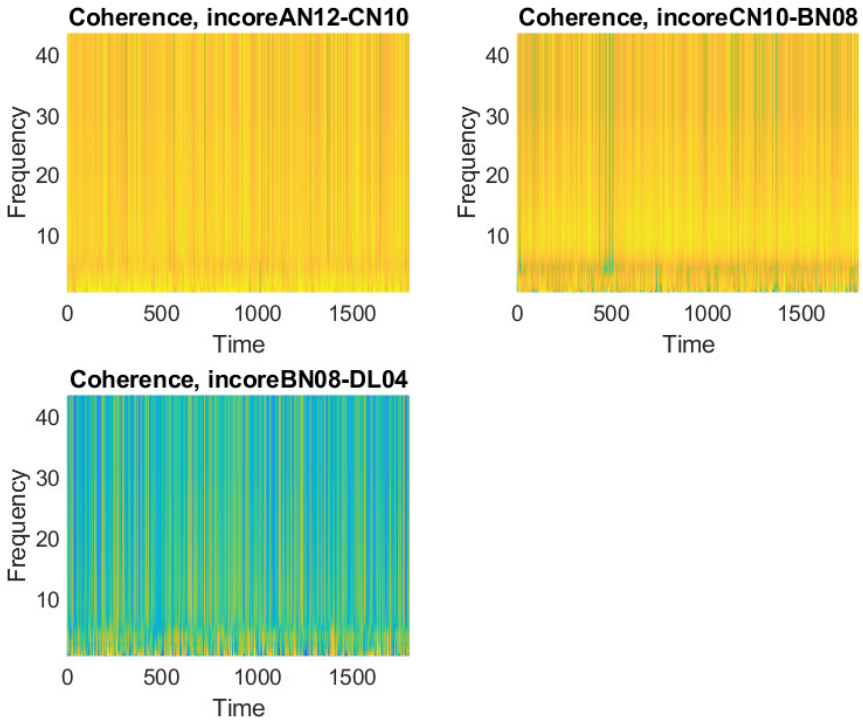

Figure 2.33: The result of the wavelet coherence of the measurement in Stage 2021, level 3, Haar wavelets

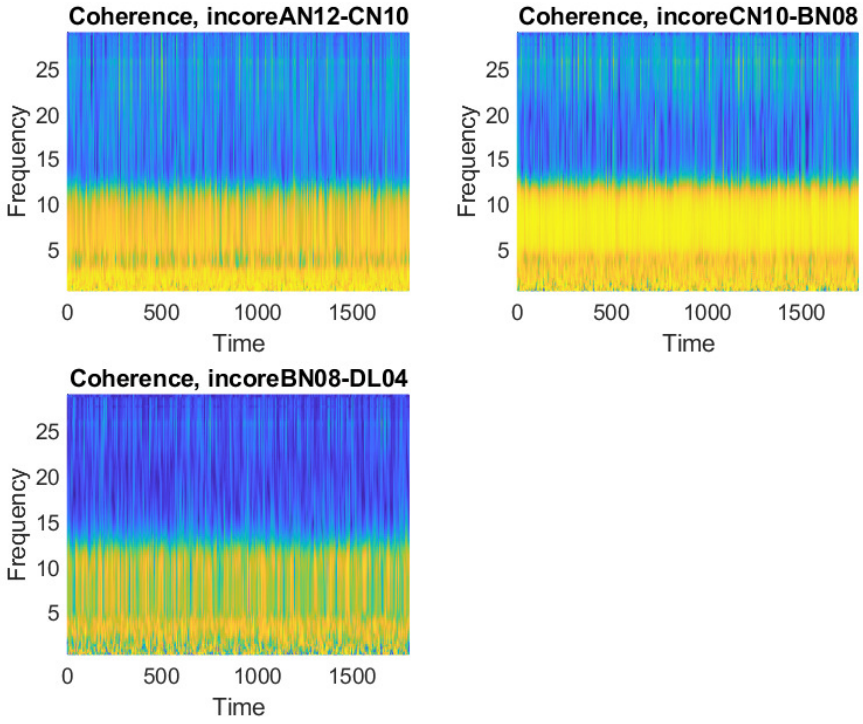

Figure 2.34: The result of the wavelet coherence of the measurement in Stage 2021, level 4, Meyer wavelets

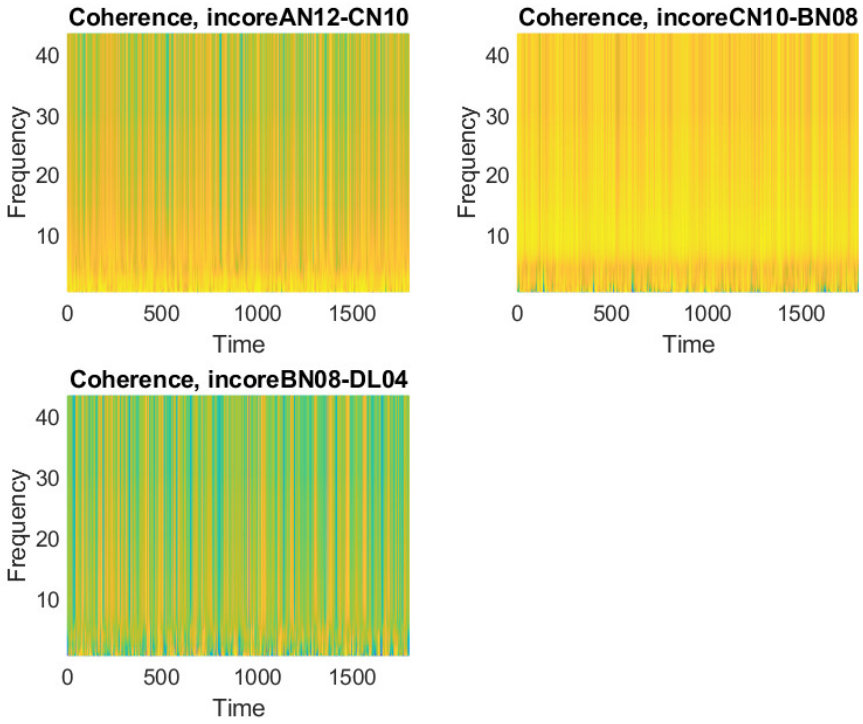

Figure 2.35: The result of the wavelet coherence of the measurement in Stage 2021, level 4, Haar wavelets

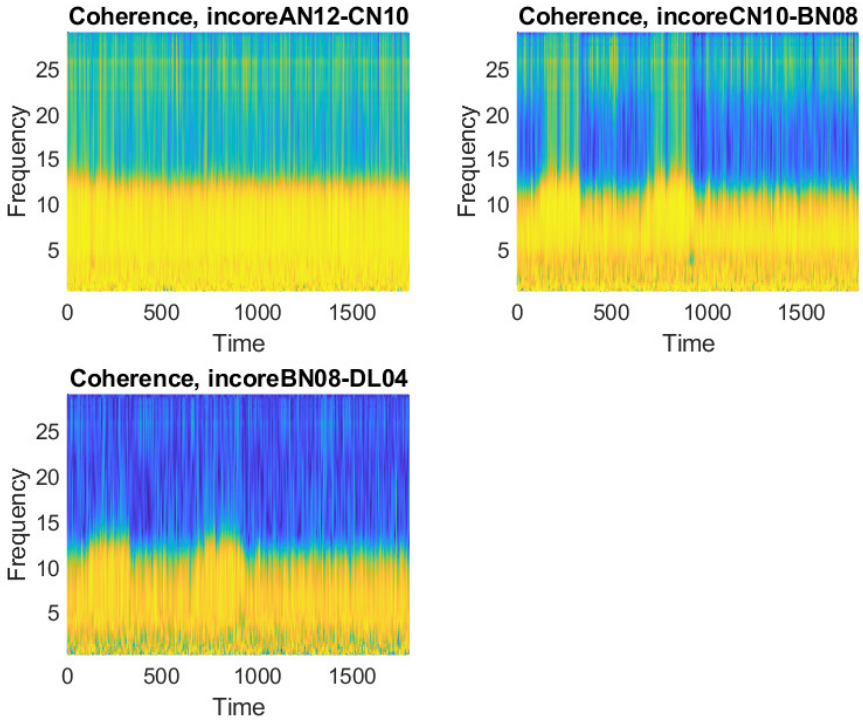

Figure 2.36: The result of the wavelet coherence of the measurement in Stage 2021, level 5, Meyer wavelets

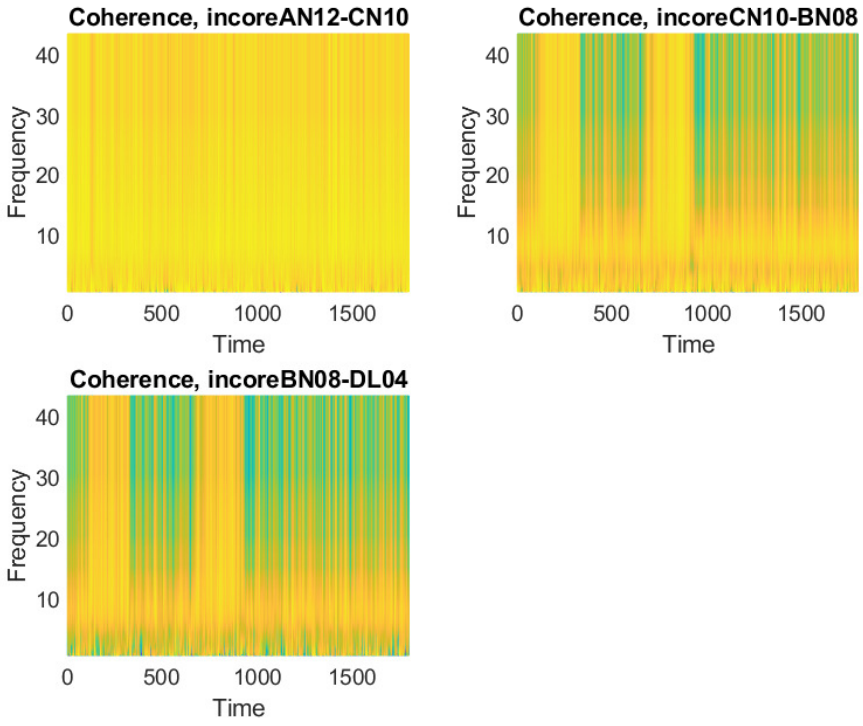

Figure 2.37: The result of the wavelet coherence of the measurement in Stage 2021, level 5, Haar wavelets

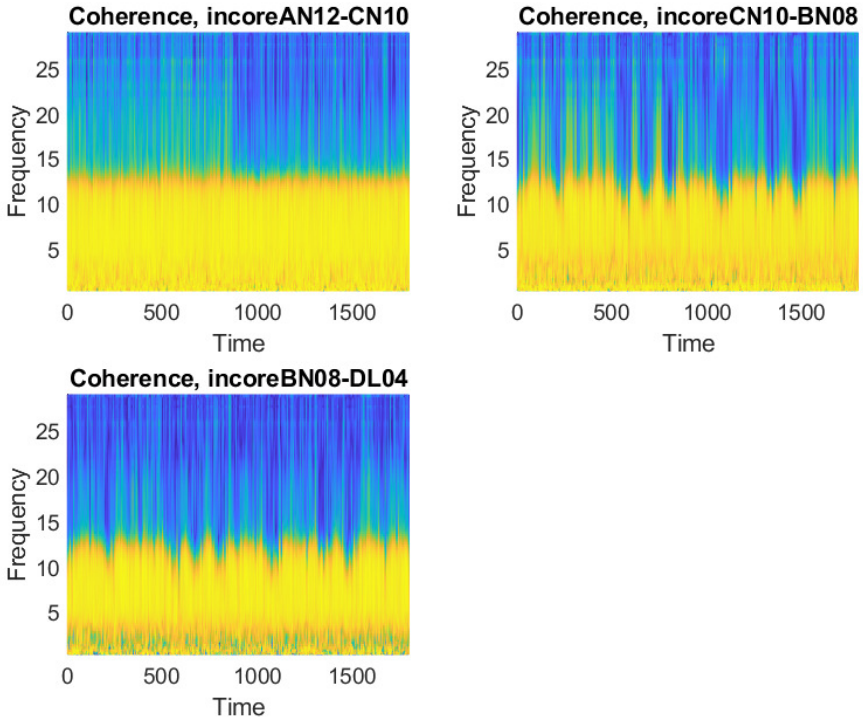

Figure 2.38: The result of the wavelet coherence of the measurement in 2021, level 6, Meyer wavelets

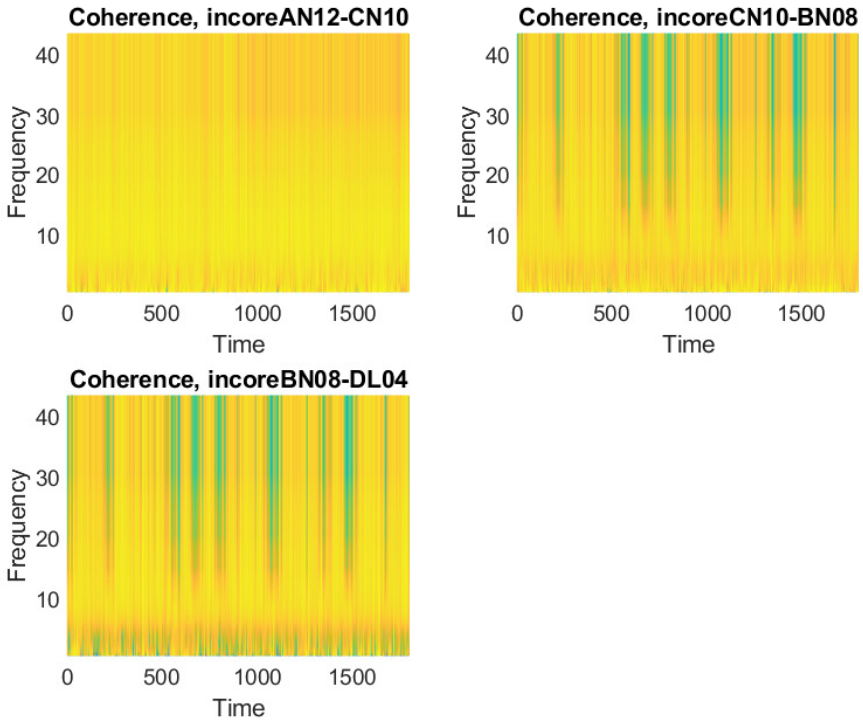

Figure 2.39: The result of the wavelet coherence of the measurement in 2021, level 6, Haar wavelets

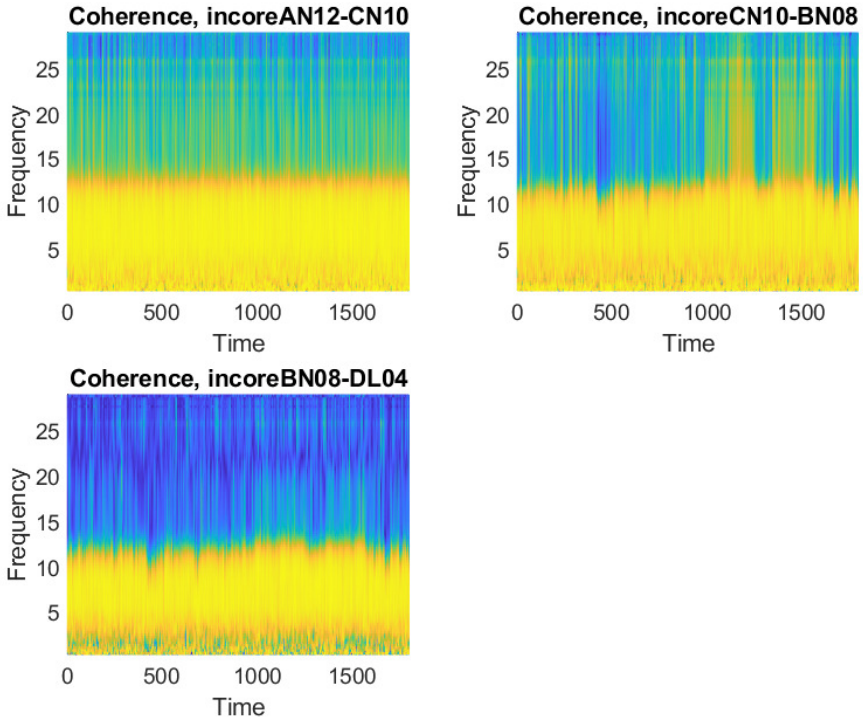

Figure 2.40: The result of the wavelet coherence of the measurement in Stage 2021, level 7, Meyer wavelets

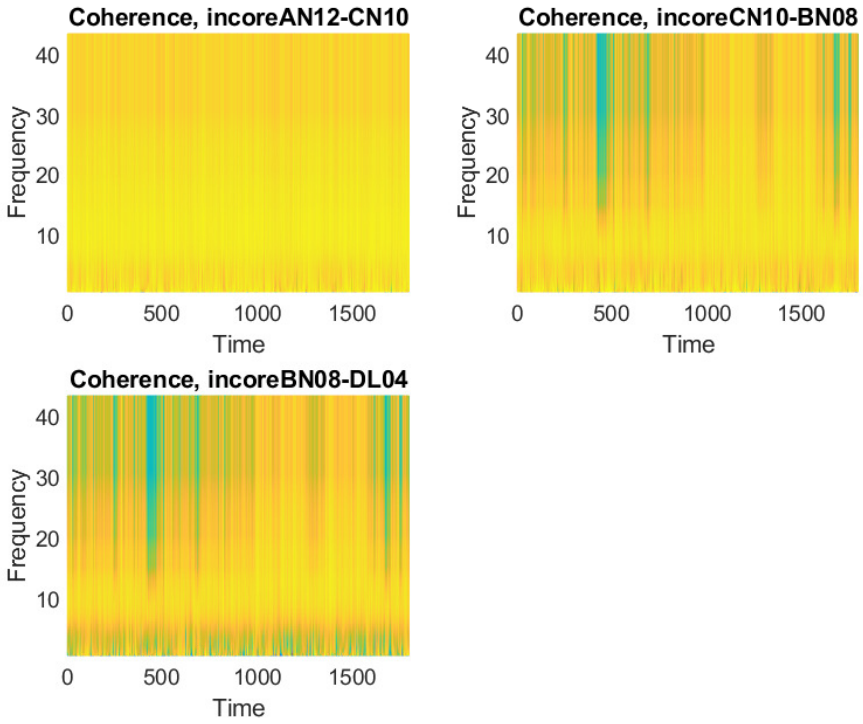

Figure 2.41: The result of the wavelet coherence of the measurement in Stage 2021, level 7, Haar wavelets

2.6 Continuous wavelet transform

In Stage 2021, a continuous wavelet transform (CWT) of Measurement 2 was made, and the results (spectrograms) were reported in the final report. In this report, for the sake of the completeness, we perform the continuous wavelet transform of the measurements made in Stage 2020 too. The results will be displayed here below. For comparison, the CWT results from Stage 2021 will also be included. The presentation will be different from that in Stage 2021, in that all four CTWs will be shown in one page, to facilitate the comparison between the fours detectors. To expedite the identification of the detectors what regards their position in the core, we will deviate from the sequence A-B-C-D, because this sequence does not correspond to the actual geometrical positioning. Instead, in one page from the bottom to the top, the figures will be shown in the sequence N12 - N10 - N08 - L04 in Fig. 2.42. This type of placing the CWTs in one page reflects the positioning of the detectors in the core, which, as mentioned earlier, is nearly on one "vertical line" on the core map, shown in Fig. 2.1.

As was already mentioned in the report of Stage 2021, and as is also seen in these time series plots, the movement of the detector from one position to the next introduces a spike in the signal around that time moment. This spike was not eliminated from the original time series of the measurement before processing the data. These spikes are visible as short time increase of the amplitude of the CWT as low frequencies, so in some way they also appear as "spikes". Although they are spike-like in the spectrogram, this is not the same as the spikes in the time series, twhich we identify as indicators of impacting. The "spikes" in the spectrogram do not carry any diagnostic information what regards impacting.

The indication of impacting could be instead associated with the occurrence of vertical structures at other times and frequencies than the above mentioned spikes, and the presence of high amplitudes in the frequency band 5 - 10 Hz, especially if several stripes can be seen An inspection of the spectrograms shows that such spike-like structures, as well as (multiple) stripes between 5 - 10 Hz can be mostly seen in the wavelet transforms of detectors A and D (N12 and L04, respectively), and to a slightly lesser extent, with detector B (N08). On the other hand, the spectrogram of detector C (N10) is to a large extent free from these indicators. This leads to the conclusion that detectors A, B and D have the highest chances to be exposed to thimble tube vibrations and impacting than detector C. This conclusion is in a good agreement with both the wavelet filtering and wavelet coherence results, as well as with the results of the measurements from 2022 (Stage 2021).

The results of the CWT analysis from Stage 2021 are shown here in order to make it easy to confirm the above statement. Since the position of the in-core detectors was the same for both Stages, the spectrograms are shown in the same order as for Stage 2020 in Fig. 2.43.

These results were already interpreted in the previous report, and we repeat these here. As mentioned there, the spectrograms makes it possible to identify the measuremet time when a certain frequency occurred, which is uniquely related to the position of the detector. As an example, in the signal of detector A (core

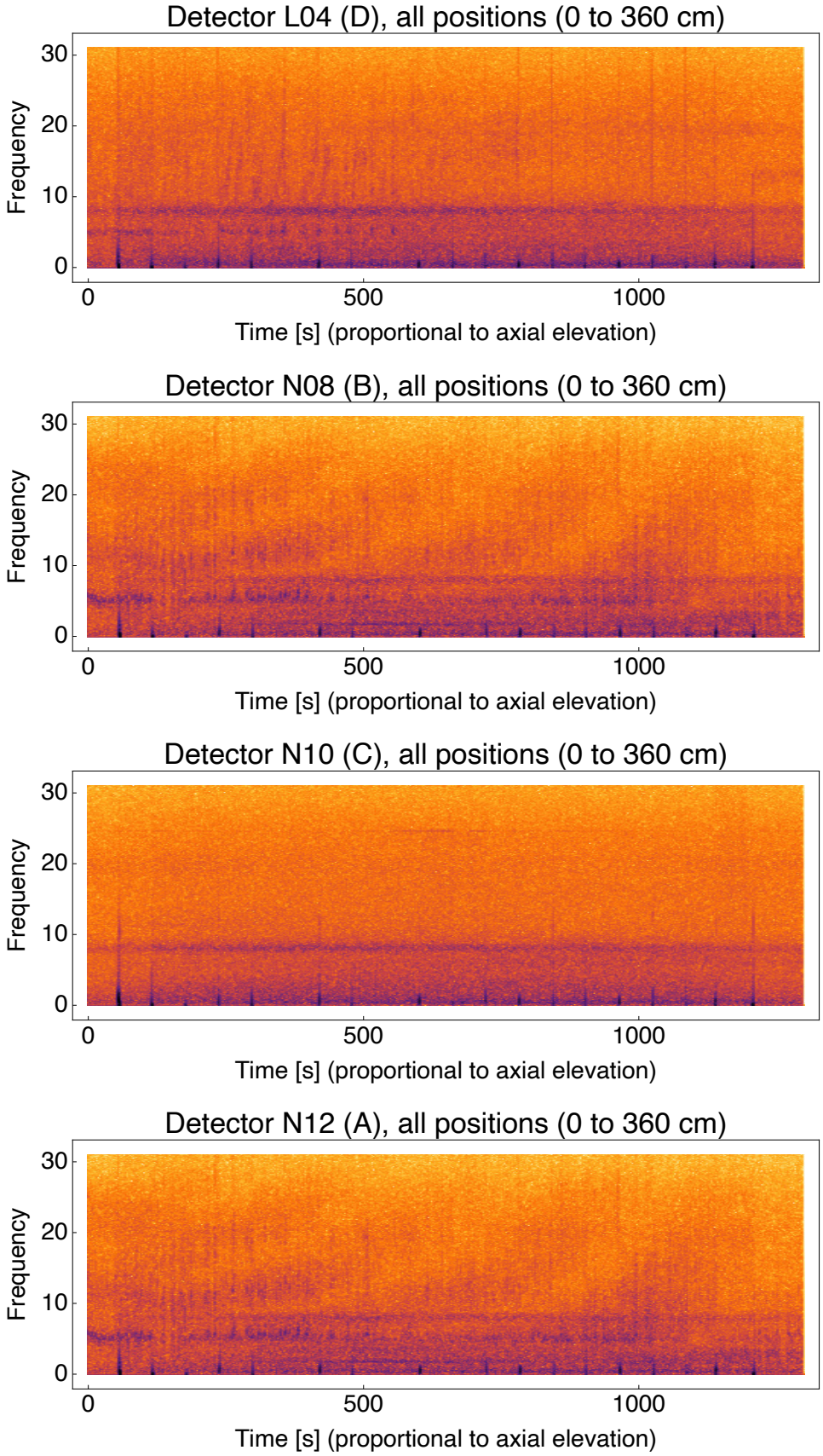

Figure 2.42: The continuous wavelet transform of the signals of detectors L04 - N12 from Measurement 2 in 2020.

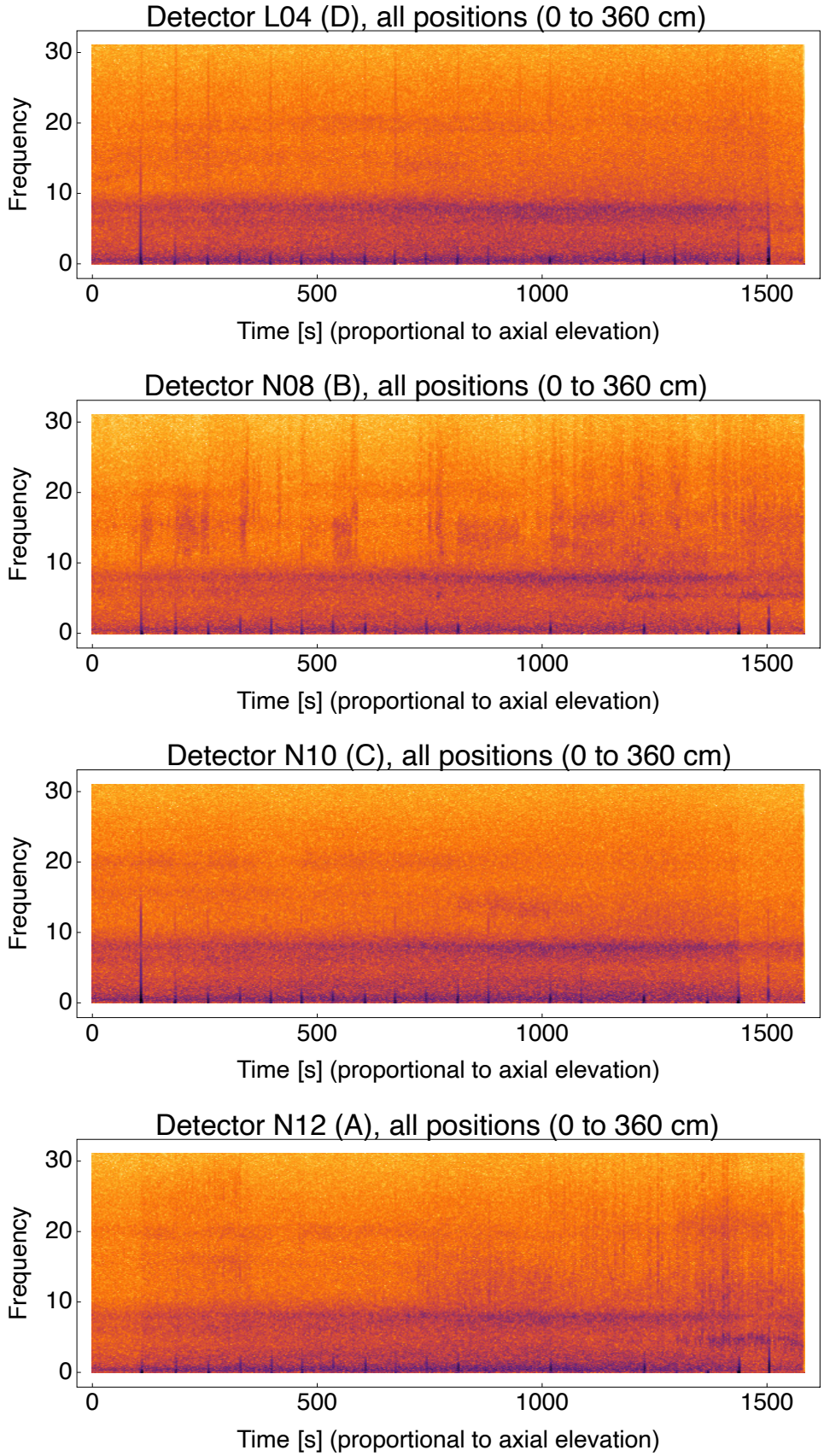

Figure 2.43: The continuous wavelet transform of the signals of detectors L04 - N12 from Measurement 2 in Stage 2021.

position N12), it is seen that the component around 5 Hz exists only at the top of the core. This is in good agreement with the analysis of Measurement 1 of Stage 2021, which also showed the peak at 5 Hz only in the position 30 cm from the top of the core. A similar effect is seen in the spectrogram of detector B (core position N08), where a component around 6 - 7 Hz appears only in the uppermost positions. In the spectrogram of detectors C and D (core positions N10 and L04, respectively), some frequencies around 15 and 20 Hz appear in part of the time.

Looking for spike-like structures in the spectrograms other than those corresponding to the movement of the detectors, one finds that such structures can be mostly seen in the wavelet transforms of detectors A and B (N12 and N08, respectively), and to a lesser extent, with detector D (L04), an finally some traces in the wavelet transform of detector C (N10). This would lead to the conclusion that detectors A and B might be exposed to thimble tube vibrations more than detectors C and D, out of the latter two D having the higher chance of impacting.

Comparing the results of the CWT analysis between Stage 2020 and Stage 2021, we find that detectors A, B and D (N12, N08 and L07) were pointed out as most likely impacting in both Stages, which is quite consistent. On the other hand, the results of the CWT are more qualitative in character than those of the wavelet filtering, and the consistency between the evaluations of the two measurements is not a guarantee that the judgements are correct. At any rate, the relatively good agreement with the wavelet filtering results increases the confidence in the overall statement about the status of thimble tube impacting.

2.7 Conclusions

At last, our previous expertise and wavelet filtering capability was restored and the tools were applied to the analysis of the measurements made in Stage 2020 and 2021. The application of the discrete wavelet based wavelet filtering method is rather straightforward, and supplies quantitative indicators that are easy to interpret. The usefulness of the wavelet coherence method, on the other hand, is much less clear. In contrast to the wavelet filtering and the pure CWT analysis, it is not performed on a single detector signal, rather its information content concerns the joint statistics of two signals. Whereas in the BWR case it could be taken between two detectors in the same detector tube, and hence it still yielded information on the individual detector tubes, here it is taken between two different detectors in two different thimble tubes at two different radial positions in the core. Since the detectors in the individual detectors may be slightly affected by vibration an impacting of thimble tubes in neighbouring fuel assemblies, the coherence might amplifiy their effect, which otherwise would not be observable in the individual detector signals. Therefore a high coherence might rather indicate vibrations and impacting in one to the thimble tubes in between two detectors, rather than in any of the two detectors. But this effect is much weaker anyway, than vibration of the thimble tubes with detectors. Accordingly, we could not draw clear conclusions from the results of the wavelet based coherence results.

Our recommendation is therefore to use primarily the discrete wavelet transform based wavelet filtering for quantification of the likelihood of impacting, and

complement the analysis with the continuous wavelet transform. The wavelet based coherence should be treated rather as a tool, whose potentials are yet to be explored and verified.

3. ACKNOWLEDGEMENT

This one-year contract was performed by funding from Ringhals Vattenfall AB, contract No. 4501756928-062. Contact person from Ringhals was Dr. Henrik Nylén.

REFERENCES

[1] J. Guitton and C. Puyal, "New trends in vibration and acoustic monitoring in nuclear components in EDF," *Progress in Nuclear Energy*, vol. 21, pp. 807–811, 1988.

[2] B. Michel and C. Puyal, "Operational and economical experience with vibration and loose parts monitoring systems on primary circuits of PWRs," *Progress in Nuclear Energy*, vol. 21, pp. 469–473, 1988.

[3] A. Trenty, C. Puyal, C. Vincent, M. H. Inchauspe, R. Baeyens, C. Messainguiral-Bruynooghe, and G. Lagarde, "Thimble vibration analysis and monitopring on 1300 and 900 MW reactors using accelerometers and in-core neutron noise (in French)," *Progress in Nuclear Energy*, vol. 21, pp. 97–106, 1988.

[4] I. Pázsit, L. A. Torres, C. Montalvo, Y. Kitamura, L. Nagy, and H. Nylén, "*Ringhals Diagnostics and Monitoring, Annual Research Report 2018-19*," CTH-NT-339/RR-22, Chalmers University of Technology, Göteborg, Sweden, June 2019.

[5] I. Pázsit and O. Glöckler, "BWR Instrument Tube Vibrations - Interpretation of Measurements and Simulation," *Annals of Nuclear Energy*, vol. 21, no. 12, pp. 759–786, 1994.

[6] C. Demazière, C. Sunde, V. Arzhanov, and I. Pázsit, "*Final Report on the Research Project Ringhals Diagnostics and Monitoring, Stage 8*," CTH-RF-177/RR-10, Chalmers University of Technology, Göteborg, Sweden, December 2003.

[7] C. Demazière, C. Sunde, and I. Pázsit, "*Final Report on the Research Project Ringhals Diagnostics and Monitoring, Stage 9*," CTH-RF-187/RR-11, Chalmers University of Technology, Göteborg, Sweden, January 2005.

[8] C. Sunde, J. Wright, C. Demazière, and I. Pázsit, "*Final Report on the Research Project Ringhals Diagnostics and Monitoring, Stage 10*," CTH-RF-194/RR-12, Chalmers University of Technology, Göteborg, Sweden, November 2005.

[9] C. Sunde, C. Demazière, and I. Pázsit, "*Final Report on the Research Project Ringhals Diagnostics and Monitoring, Stage 11*," CTH-NT-206/RR-13, Chalmers University of Technology, Göteborg, Sweden, February 2007.

[10] I. Pázsit, C. Demazière, C. Sunde, P. Bernitt, and A. Hernández-Solís, "*Final Report on the Research Project Ringhals Diagnostics and Monitoring, Stage 12*," CTH-NT-220/RR-14, Chalmers University of Technology, Göteborg, Sweden, August 2008.

[11] I. Pázsit, N. S. Garis, J. Karlsson, and A. Rácz, "*Forskningsprogram angående härddiagnostik med neutronbrusmetoder Etapp 3. Slutrapport*," SKI Rapport 97:31, SKI, September 1999.

[12] I. Pázsit, C. Demazière, V. Arzhanov, and N. S. Garis, "*Research and Development Program in Reactor Diagnostics and Monitoring with Neutron Noise Methods Stage 7. Final Report*," SKI Rapport 01:27, SKI, August 2001.

[13] I. Pázsit, C. Demazière, and V. Arzhanov, "*Research and Development Program in Reactor Diagnostics and Monitoring with Neutron Noise Methods Stage 8. Final Report*," SKI Rapport 2003:08, SKI, January 2003.

[14] I. Pázsit, "*Ringhals Diagnostics and Monitoring: An overview of 30 years of collaboration 1993 - 2023*," CTH-NT-350/RR-27, Chalmers University of Technology, Göteborg, Sweden, June 2023.

[15] J. Thie. Personal communication on the 18th IMORN, Prague, Czechoslovakia, 1985.

[16] A. Rácz and I. Pázsit, "Diagnostics of detector tube impacting with wavelet techniques," *Annals of Nuclear Energy*, vol. 25, no. 6, pp. 387–400, 1998.

[17] I. Pázsit and O. Glöckler, "On the Neutron Noise Diagnostics of Pressurized Water Reactor Control Rod Vibrations II. Stochastic Vibrations," *Nuclear Science and Engineering*, vol. **88**, pp. 77–87, 1984.

[18] I. Pázsit and O. Glöckler, "On the Neutron Noise Diagnostics of Pressurized Water Reactor Control Rod Vibrations III. Application at a Power Plant," *Nuclear Science and Engineering*, vol. 99, no. 4, pp. 313–328, 1988.

[19] I. Pázsit, L. A. Torres, C. Montalvo, L. Nagy, G. Klujber, M. Szieberth, T. Misawa, Y. Kitamura, V. Dykin, and H. Nylén, "*Ringhals Diagnostics and Monitoring, Annual Research Report 2020-21*," CTH-NT-344/RR-24, Chalmers University of Technology, Göteborg, Sweden, June 2021.

[20] P. S. Addison, *The Illustrated Wavelet Transform Handbook*. Bristol: Institute of Physics Publishing, 2002.

[21] G. Pokol and G. Por, "Surveillance of vibrations in PWR," *International Journal of Nuclear Energy Science and Technology*, vol. **2**, pp. 241–252, 2006.

CHALMERS UNIVERSITY OF TECHNOLOGY
SE 412 96 Gothenburg, Sweden
Phone: + 46 - (0)31 772 10 00
Web: www.chalmers.se